VOL. 16 No. 3, pp. 69-104 SEPTEMBER 1954

Philips Technical Review

DEALING WITH TECHNICAL PROBLEMS
RELATING TO THE PRODUCTS, PROCESSES AND INVESTIGATIONS OF
THE PHILIPS INDUSTRIES

EDITED BY THE RESEARCH LABORATORY OF N.V. PHILIPS' GLOEILAMPENFABRIEKEN, EINDHOVEN, NETHERLANDS

FUNDAMENTALS OF THE GAS REFRIGERATING MACHINE

by J. W. L. KÖHLER and C. O. JONKERS.

621.573

A hot-air engine suddenly deprived of heat from its burner, but kept in motion by an electric motor, functions as a refrigerator ("gas refrigerating machine"). In this sense it is entirely analogous to the steam engine which, although perhaps not widely known, functions as a (compression) refrigerator if the process of heating is discontinued and motive power is supplied from outside to keep the engine turning: the water in the boiler then cools rapidly and finally reaches a temperature below that of the surrounding atmosphere (the pressure in the condenser becomes higher than that in the boiler). It will be noted, however, that whereas the steam engine and the compression refrigerator have developed along entirely different lines, a gas refrigerating machine can be designed on principles very closely related to those of the hot-gas engine. This is substantiated by the theoretical arguments contained in this article, and will be further elucidated in a subsequent article dealing with the gas refrigerating machine recently developed at Philips.

Although even in primitive times man was able to heat objects (the knowledge of fire dates back to the very beginnings of the stone age), thousands of years elapsed before he learned how to effect cooling to temperatures below that of the surrounding atmosphere. The Egyptians are known to have kept their beverages cool by storing them in porous vessels, but ice could not be obtained even in Roman times by any means other than by fetching it from some natural source, often a distant mountain. Machines for generating "cold" were described for the first time during the nineteenth century.

The late development of methods of effecting cooling may be related to the fact that it is very much less essential to human life than heating. However this may be, it is certainly also largely attributable to the appreciably greater complexity of methods of producing cold. Methods of generating heat are legion and require no enumeration; on the other hand, only a few — usually complex — methods of generating cold are known even at the present time, and only a few of these are applied in practice. Some of these methods are outlined below.

Probably the oldest, and still the most widely used method of effecting a decrease in temperature is cooling by evaporation. A liquid is allowed to evaporate, and the vapour is removed, so that no state of equilibrium can be reached; the evaporation thus continues without interruption. Heat is absorbed by the evaporation process and the liquid therefore cools. The simplest example of this process is the sensation of cooling perceived when a moistened finger is held in the wind; another is the use of porous vessels which, as we have already seen, effect cooling by the gradual evaporation of liquid through the porous walls. In machines that operate continuously on this principle, the vapour (the refrigerant) is restored to the liquid phase usually by pumping and compressing the vapour; machines which do this are compression refrigerators. The absorption refrigerator is another type based on cooling by evaporation.

The lowest temperature economically attainable with these refrigerators depends primarily upon the decrease in the vapour pressure of the particular refrigerant with the temperature; the great volume of vapour to be pumped in the case of a low vapour pressure would necessitate the use of a very large machine. For this reason, temperatures below about −60 °C to —80 °C cannot be attained with such refrigerators, despite the use of modern refrigerants. These temperatures are low enough, e.g. for the production of solid carbon dioxide ("dry ice", sublimation point —78 °C at 1 atm.), a process nowadays widely used for storing and conveying cold to places where it is needed (refrigerative containers) — in the same way as with ordinary ice. To obtain temperatures below —80 °C with an evaporation refrigerator, two or more cyclic processes, each involving a different refrigerant must be linked together; this "cascade method" was used at one time but is now almost completely obsolete, owing to its complexity.

There is another, very much lower range of temperatures which is now frequently and relatively easily attained by means of machines operating on quite different principles. This is the range associated with liquid air, the boiling point of which is —194 °C at 1 atm. (*fig. 1*). The liquefaction of air on a commercial scale was first accomplished by Carl von Linde. He employed the Joule-Kelvin effect that is, the decrease in temperature that takes place in all gases below a certain temperature when passed through an orifice from a high to a low pressure. Another method of producing a decrease in temperature was used shortly afterwards by Claude, this being the adiabatic expansion of compressed air with the performance of mechanical work. Modern equipment for the production of liquid air embodies a combination of these two methods.

The range of temperatures between about —80 °C and —180 °C, is at present virtually unexploited; there are few simple machines working within this range.

Naturally, this brief survey is far from complete. In particular, it fails to reflect the great increase in the use of refrigeration ever since the first continuously operated machines were designed. The development of new applications continues and the introduction of new refrigerating techniques can be expected to lead to still further applications. The development described below should be regarded in this light. In proceeding to this description, we shall refer to a series of articles on hot-air engines published in this Review a few years ago [1]). In the first of these it was stated that the hot-air cycle described could also be used for refrigeration, and that very low temperatures could, in fact, be attained in this way. Investigations carried out during recent years have shown that refrigerators based upon this "gas refrigeration cycle" can exhibit particularly favourable properties precisely within the unexploited range between —80 °C and —180 °C. In fact, the gas refrigerating machine reaches this range in one stage from room temperature, thus considerably simplifying the equipment.

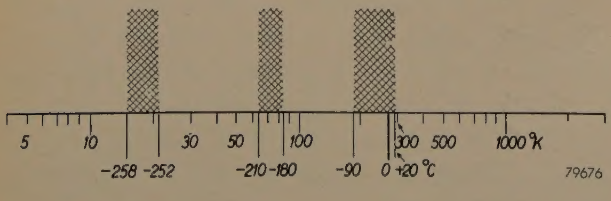

Fig. 1. Temperature ranges covered by conventional refrigerators and liquefiers. Evaporation type refrigerators normally go down to about —80 °C. The equipment used for the liquefaction of air operates in the range —180 °C to —210 °C. Hydrogen liquefiers operate between —252 °C and —258 °C.

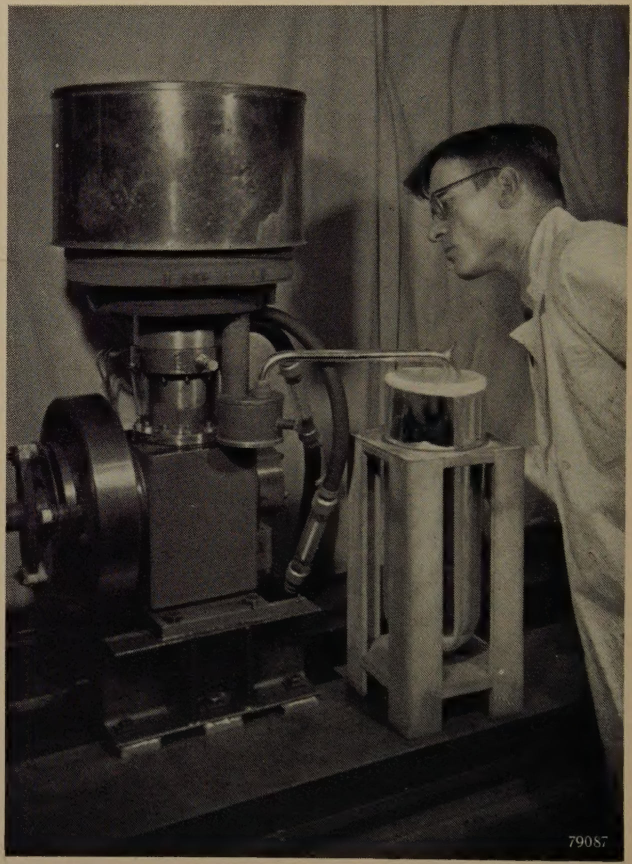

Fig. 2. Gas refrigerating machine used for the liquefaction of air in the Philips Laboratories at Eindhoven.

Machines of this type, capable of generating cold very efficiently at still lower temperatures, e.g. —200 °C, can also be designed. This is demonstrated by the refrigerating machine illustrated in *fig. 2*, constructed in the Philips Laboratories at Eindhoven, which is capable of liquefying air at atmospheric pressure. In this process the air to be liquefied need not be compressed. This fact permits some surprising simplifications, which have led to an extremely compact apparatus requiring very little attention.

---

[1]) H. Rinia and F. K. du Pré, Air engines, Philips tech. Rev. **8**, 129-160, 1946.
H. de Brey, H. Rinia and F. L. van Weenen, Fundamentals for the development of the Philips air engine, Philips tech. Rev. **9**, 97-124, 1947.
F. L. van Weenen, The construction of the Philips air engine, Philips tech. Rev. **9**, 125-160, 1947.
The hot-air engine is more appropriately named *hot-gas engine*, since the working fluid is not restricted to air.

In this article the fundamentals of the gas refrigeration cycle will be discussed. The practical limitations of this cycle and the design of the actual machine with be dealt with in a second article.

The gas refrigeration cycle

In gas refrigeration, a quantity of gas is compressed at room temperature and the heat of compression thus generated is dissipated, e.g. by cooling-water. Next, the gas is cooled to the desired low temperature (it is assumed that the steady state has been reached, i.e. that a region of the machine is already cooled to this particular temperature), and it is permitted to expand with the performance of mechanical work. The cold of expansion 2) thus liberated is the essence of the entire process. Finally, the expanded gas is re-heated to room temperature and another cycle is commenced.

In principle, then, the process may be divided into four phases:

I. Compression of the refrigerant at the ambient temperature.
II. Cooling to the working temperature.
III. Expansion at the working temperature, with a consequent generation of cold (absorption of heat).
IV. Re-heating to the ambient temperature.

The refrigerant, unlike that in evaporation refrigerators, remains gaseous throughout this process. Since a *closed system* is used, the choice of refrigerant is not restricted to air; any other refrigerant may be used, provided that its behaviour approximates sufficiently well to that of a perfect gas.

It will be seen that the gas refrigeration process is somewhat similar to the Claude process mentioned in the introduction. In both processes gas is compressed at room temperature and allowed to expand at the working temperature. The object of the Claude process, however, like that of the Linde process, is to extract the cooled and liquefied gas from the system, whereas in gas refrigeration the gas merely acts as the working fluid (analogous to the liquid in the evaporation refrigerator). Moreover, the practical forms of these two processes differ so considerably that there is little to be gained by comparing them.

The process outlined here was at one time carried out by means of two separate machines, one for compression and one for expansion (in this form it is known in the literature as the air refrigeration process). However, a single machine containing two compartments in communication with each other but at different temperatures can also be used; the refrigerator then contains no valves and is therefore extremely simple. This type of machine is similar to the well-known Stirling air engine. The operation of the Philips gas refrigeration cycle will first be discussed in terms of a schematic cycle in which the four distinct phases of the cycle can be identified. This schematic process is not suitable for practical application, since it involves a discontinuous movement of pistons, but it will be shown in due course that an equivalent cycle can be obtained with a *continuous* piston movement.

Schematic cycle

Fig. 3a shows a cylinder containing two pistons; the one on the right moves in a region of the cylinder which is at high temperature T_C, i.e. at room temperature (about 300 °K), and the one on the left in another region of the cylinder at a low temperature (T_E). Between the two portions is a regenerator R (heavy dotted line), the purpose of which is described in the next section. In phase *I* of the cycle (the transition *1*→*2* in the diagram) the gas is compressed at temperature T_C (C = compression) from volume V_1 to volume V_2. It is assumed that the compression is isothermal, i.e. that the heat of compression is removed from this

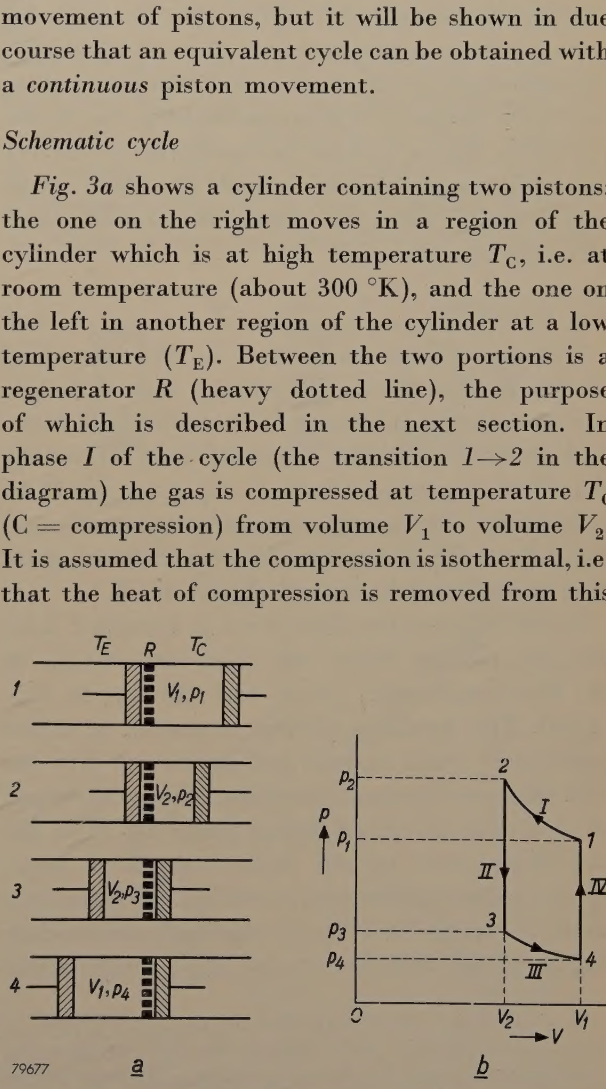

Fig. 3. The schematic cycle of the gas refrigeration process. *a*) Two pistons move in a cylinder, one region of which is at room temperature (T_C), another region (the freezing space) being at a low temperature (T_E). A regenerator (R) is situated between these two regions. The process comprises four phases *I-IV*, the initial states (*1-4*) of which are shown in the diagram.
b) Variation in the pressure and volume of the working fluid. Phases *I* and *III* of the cycle are isothermal, phases *II* and *IV* are isochoric (constant volume).

---

2) Reference to the generation of "cold" in the qualitative sense has already been made in the earlier part of this article. Following the accepted usage of refrigeration terminology, we shall now apply the same term quantitatively; thus the production of a quantity of cold by a working fluid simply means the absorption of a quantity of heat by the fluid from its surroundings.

part of the cylinder. In phase *II* of the cycle ($2 \rightarrow 3$) the gas is transferred without change in volume to the low-temperature (T_E) region of the cylinder (left); the decrease in temperature of the gas during this phase causes a drop in pressure. In phase *III* ($3 \rightarrow 4$) the gas expands at temperature T_E (E = expansion) from volume V_2 to the original volume V_1, whereupon the pressure diminishes still further, and heat is absorbed from the surroundings of this region of the cylinder. In the final phase *IV* ($4 \rightarrow 1$) the gas is transferred isochorically (at constant volume) back to the right hand section of the cylinder which is at room temperature (T_C). During this process the pressure increases and condition *I* is restored. The whole process thus consists of passing the same quantity of gas to and fro between the two temperature regions at T_C and T_E, compressing it in the former and expanding it in the latter. In the *p-V* diagram shown in fig. 3*b*, the process is defined by the two isotherms *I* and *III* and the two isochores *II* and *IV*. The actual absorption of heat, i.e. production of cold, takes place during phase *III*.

The regenerator

The regenerator mentioned in the preceding section is essential to the process, since if the gas compressed during phase *I* at temperature T_C were to pass direct into the space at temperature T_E, the effective output of cold on expansion would be reduced by the amount necessary to cool the gas from T_C to T_E; in fact this loss would be so great that there would be no real output at all.

In the regenerator, then, heat is extracted from the gas passing from the high-temperature to the low-temperature space, and the gas is thus cooled. The quantity of heat extracted is stored temporarily (that is, it is not discharged into the cold space and does not, therefore, reduce the output of cold). On returning during phase *IV* from the low-temperature to the high-temperature zone, the gas re-absorbs the heat stored in the regenerator; hence it enters, and leaves the high-temperature region of the cylinder at the same temperature.

In view of the essential function of the regenerator it is important to recognize that, theoretically, 100% regeneration is possible. This may be shown as follows. The heat energy transferred from the gas to the regenerator in phase *II*, as well as the heat energy transferred to the gas from the regenerator in phase *IV*, are given by

Energy = mass × temp. difference × specific heat.

Since we are considering a closed system, the mass of the working fluid is the same in both phases. The temperature difference is also the same in each case. Furthermore, the specific heat remains constant although the average pressure is greater during phase *II* than during phase *IV*, for we are here considering perfect gases whose specific heats are independent of pressure. Hence the heat transferred from the gas to the regenerator in phase *II* is equal to that transferred to the gas from the regenerator in phase *IV*.

In practice, of course, the regenerator does not achieve 100 % regeneration, but it nevertheless drastically reduces the loss of cold in phase *II*. For the present we shall proceed on the assumption that the refrigerator considered is provided with an ideal regenerator, i.e. that this loss may be ignored.

Energy balance in the schematic process

It can be shown (see below, small type) that the quantity of cold produced per cycle in the expansion cylinder is given by

$$Q_E = mRT_E \ln \frac{V_1}{V_2}, \quad . \quad . \quad . \quad . \quad . \quad (1)$$

and that the mechanical work which has to be performed per cycle is

$$W = mRT_C \ln \frac{V_1}{V_2} + mRT_E \ln \frac{V_2}{V_1} =$$

$$= mR(T_C - T_E) \ln \frac{V_1}{V_2}. \quad . \quad . \quad (2)$$

In these formulae, R is the gas constant and m the mass (in gram-molecules) of the working fluid.

It will be seen that both Q_E and W are proportional to the logarithm of the volume ratio V_1/V_2, and to the quantity of gas present in the system; W is positive, i.e. there is a net surplus of work to be performed (also shown by the *sense* of the cycle indicated in the *p-V* diagram, fig. 3*b*). It will also be seen that Q_E is proportional to T_E; hence the output of cold decreases as the temperature of the freezing-space decreases. But the required mechanical work is proportional to the temperature difference $T_C - T_E$; it is thus zero when $T_C = T_E$, and increases steeply according as T_E decreases.

The refrigeration "efficiency", or better, the "coefficient of performance", is the ratio between the cold produced and the mechanical work expended. Applying formulae (1) and (2), we find that this ratio is:

$$\eta = \frac{Q_E}{W} = \frac{T_E}{T_C - T_E}.$$

This corresponds to the thermal efficiency of the Carnot cycle which, according to thermodynamics, is the highest efficiency attainable in a cycle operating between temperatures T_C and T_E. To attain this efficiency the cycle must be reversible; provided that the assumptions of isothermal compression and expansion and perfect regeneration are valid, the present process satisfies this condition. It is seen that the efficiency decreases sharply as the temperature of the cold region of the machine is lowered (*fig. 4*). On the other hand it is seen — and the same applies in principle to all refrigerators — that the efficiency exceeds unity when the temperature difference $T_\mathrm{C} - T_\mathrm{E}$ is small, and even becomes infinite in the extreme case where $T_\mathrm{C} \to T_\mathrm{E}$.

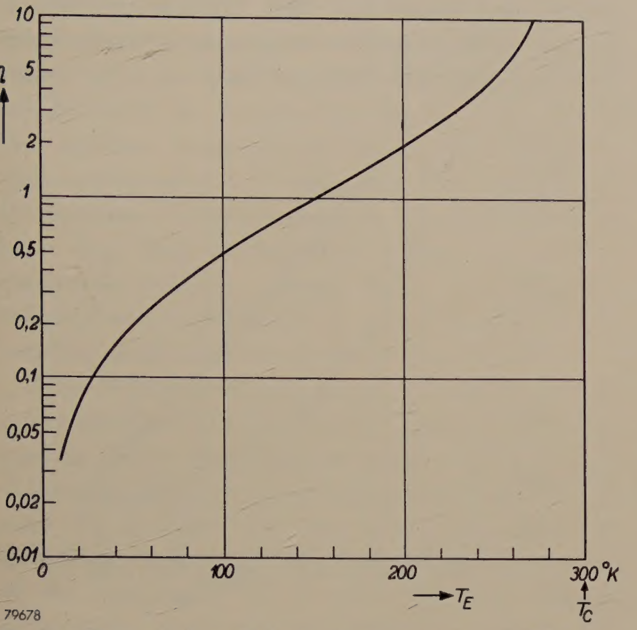

Fig. 4. Theoretical coefficient of performance η of the gas refrigeration cycle (i.e. thermal efficiency of Carnot cycle, $\eta = \dfrac{T_\mathrm{E}}{T_\mathrm{C} - T_\mathrm{E}}$) plotted against the freezing-temperature T_E, for an ambient temperature $T_\mathrm{C} = 300$ °K.

For this reason the term "coefficient of performance" is to be preferred to "efficiency" for the ratio Q_E/W. The latter suggests that a certain percentage of the required mechanical work is converted into the desired product ("cold"), whereas in reality the cold is produced by *transferring* ("pumping") heat from a low-temperature, to a high-temperature reservoir, the mechanical work merely being used to drive the "pump".

Formulae (1) and (2) may be derived briefly as follows. The work done by a piston in compressing a certain quantity of gas in a cylinder at a pressure p is

$$W = -\int p\,\mathrm{d}V,$$

where $\mathrm{d}V$ is the change in volume. For the mass of gas considered here, we have, from the gas laws:

$$W = -mRT\int\frac{\mathrm{d}V}{V}.$$

Thus the work performed by the piston of the compression cylinder in phase *I* of the schematic cycle corresponds to:

$$W_\mathrm{I} = -mRT_\mathrm{C}\int_{V_1}^{V_2}\frac{\mathrm{d}V}{V} = mRT_\mathrm{C}\ln\frac{V_1}{V_2},$$

which is converted into heat of compression. Similarly, we have for the expansion cylinder in phase *III*:

$$W_\mathrm{III} = -mRT_\mathrm{E}\ln\frac{V_1}{V_2} \quad\text{and}\quad Q_\mathrm{E} = RT_\mathrm{E}\ln\frac{V_1}{V_2}.$$

Formulae (1) and (2) follow direct from the above.

It will be noted that the pressure of the working fluid changes also during phases *II* and *IV*; the pressure (in both cylinders) decreases during phase *II* and increases during phase *IV*, with the result that the fluid has to absorb heat from the cylinder walls in the former, and give up heat to the walls in the latter phase. However, since the pressure ratio in phase *II* is equal the pressure ratio in phase *IV*, and since the quantity of heat transferred depends only on the pressure ratio, the heat absorbed by the fluid in each of the two cylinders during phase *II* is equal to the heat given up during phase *IV*; hence the two terms cancel each other out in the energy balance.

Process based on continuous piston movement

As already mentioned, the schematic cycle described above is unsuitable for practical application by reason of the discontinuous piston movement involved.

As can be seen from *fig. 5*, however, an approximation to this cycle can be achieved by a *harmonic* movement of the pistons. It is then necessary to introduce a phase displacement between the movements of the two pistons, such that *the change in volume in the expansion cylinder is given a phase*

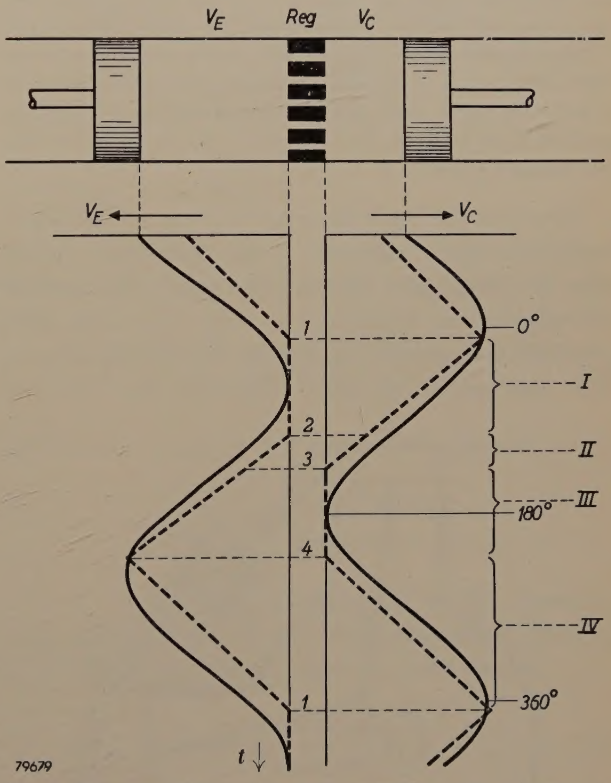

Fig. 5. The gas refrigeration cycle operating with a harmonic piston movement. The variation of V_C (volume of room-temperature region) and V_E (volume of low-temperature region) are plotted against time *t*. The dotted line represents the corresponding variation in the schematic process (non-harmonic piston movement). This diagram also shows that the regenerator (*Reg*) has a finite volume of its own (see fig. 6) which, together with other spaces not swept out by the pistons, represents a "dead space". This reduces the pressure variation in the refrigerator and thus also the refrigerating capacity, but does not affect the efficiency of the process.

lead with respect to the corresponding volume change in the compression cylinder. Fig. 6 shows that a simple drive can be used to impart the required movement to the two pistons (another method, which has certain advantages over this, will be described in the second article). In the case of a harmonic piston movement, the *p-V* diagram becomes a smooth continuous curve (*fig. 7*), which implies a merging of the four phases *I-IV*. Compression still takes place mainly — but not entirely — at temperature T_C; similarly, expansion is not confined exclusively to temperature T_E. Moreover, some change of volume now occurs during phases *II* and *IV*, i.e. the isochoric character of the gas transfer is lost. The more important properties of the cycle thus obtained will be discussed in the remainder of this article. A more thorough analysis (which is beyond the scope of this article) shows that the usefulness of the cycle is not lost when a harmonic piston movement is employed.

The fact that the isochoric character of phases *II* and *IV* is not essential may be seen as follows. The cycle may equally well be schematised by a discontinuous piston movement involving an *isobaric* (constant pressure) instead of an isochoric transfer of the gas during phases *II* and *IV*. The conclusions already reached remain valid also in this case. In many ways, the practical form of the cycle based on a harmonic piston movement may be considered as an intermediate form between that with the isochoric and that with the isobaric phases.

Now that the basic theory of the gas refrigeration cycle has been outlined, a few historical details may be given. Like the hot-air engine, this method of refrigeration originated a long time ago. The possibility of generating cold by the Stirling process was conceived by John Herschel in 1834. A patent for a machine operating on this principle was granted to Alexander Kirk [3]) in 1862; this machine was in use for more than a decade. More recently Lungaard in the U.S.A. worked on a refrigerator based on the Stirling process. It appears that very low temperatures have never been attained with these machines.

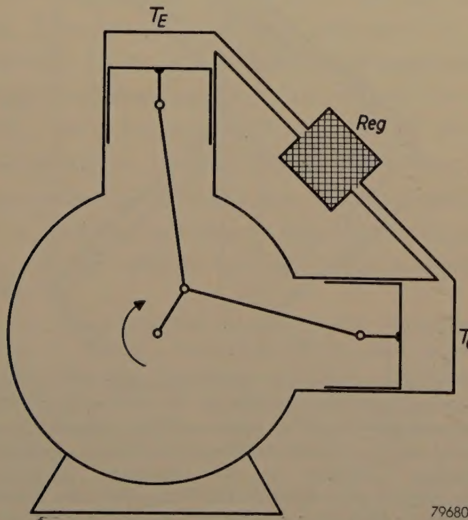

Fig. 6. Crank drive which can be used to produce a harmonic piston movement with the required phase displacement. In the case shown, the phase angle between the volume variations of the compression and expansion spaces is 90°.

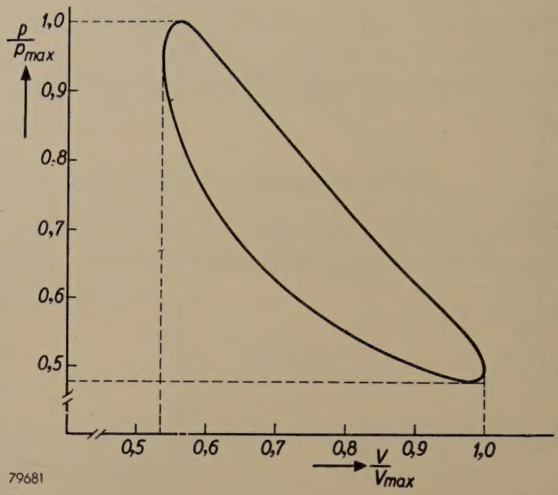

Fig. 7. *p-V* diagram for the gas refrigeration cycle operating with a harmonic piston movement. The phases *I-IV* of the cycle merge to some extent; hence a smooth envelope is obtained instead of the discontinuous diagram shown in fig. 3*b*.

Relationship between the gas refrigerating machine and the hot gas engine

Comparing the gas refrigerating machine described above, with the hot-gas engine as described in the first of the articles referred to in [1]), their close resemblance in principle will at once be noted. In view of their quite different purposes, however, they should be regarded from different points of view.

The gas refrigeration cycle is frequently referred to as the "hot-air cycle in reverse", but because this phrase is so easily misinterpreted, we shall now proceed to a closer examination of the relationship between the two machines.

Consider first the operation of the hot-gas engine. Its cycle is entirely analogous to that demonstrated in fig. 5, but in the engine the temperature T_E of the expansion cylinder is kept high, e.g. 600 °C; the other cylinder is again at the ambient temperature T_C. In these circumstances, i.e. when heat is supplied to the expansion cylinder at temperature T_E and the other cylinder at T_C is cooled, the engine delivers mechanical power to the shaft. If the heating of the expansion cylinder is discontinued, but the machine is maintened in rotation at the same speed and in the same direction (by applying power from outside), the change will not be detected by the interior of the machine, since the working fluid will continue to go through the same cycle as before; hence the fluid will continue to absorb heat from the expansion cylinder. Deprived of its source of heat, this cylinder will therefore cool rapidly until its temperature finally drops below the ambient temperature; the hot-air engine is thus converted into a refrigerator. The decrease in temperature continues until the residual influx of heat (e.g. due to imperfect insulation) to the expansion cylinder, cooled below the ambient temperature, is balanced by the rate of heat absorption (cold output) of the working fluid.

---

[3]) A. G. Kirk, Min. Proc. Inst. Civ. Eng. **37**, 244, 1873/74.

Thus in both the hot-gas engine and the gas-refrigerating machine, heat is absorbed from outside by the working fluid in the expansion cylinder. The principal difference between the two machines lies in the temperature T_E at which this absorption takes place: in the engine T_E is higher than the ambient temperature: in the refrigerator T_E is lower than the ambient temperature. Both machines, however, rotate in the same direction and with a phase difference of the same sign between the two piston movements [4].

Performance calculations on the cycle based on harmonic piston movement

The calculation of cold output, mechanical power (shaft power) and coefficient of performance, outlined above for the schematic cycle of the Stirling process, may now be made for the cycle involving a harmonic piston movement. From what has already been said it will be clear that the calculation will be substantially the same as that previously described for the hot-air engine, provided that the quantities employed are suitably defined.

The following notation will be used:

V_E, T_E = volume and absolute temperature of the expansion space (referred to in the articles of [1]) as the hot space of the hot-air engine, with suffix *h*).

V_C, T_C = volume and absolute temperature of the compression space (referred to in the articles of [1]) as the cold space of the hot-air engine, with suffix *c*).

V_0 = maximum value of V_E.

wV_0 = maximum value of V_C.

τ = T_C/T_E, the temperature ratio of the machine; for the engine $\tau<1$ and for the refrigerator $\tau>1$.

V_s = volume of the dead space, that is the total volume of the circulation system other than that of the cylinders proper.

T_s = absolute temperature of the dead space (average for this space),

s = $\dfrac{V_s}{V_0}\cdot\dfrac{T_C}{T_s}$, the relative reduced dead space.

Assuming that the variation of V_E and V_C is harmonic, we write:

$$\left.\begin{aligned} V_E &= \tfrac{1}{2} V_0 (1+\cos\alpha) \\ \text{and}\quad V_C &= \tfrac{1}{2} w V_0 [1+\cos(\alpha-\varphi)] \end{aligned}\right\} \quad . \; . \; (3)$$

where

α = the crank angle of the machine, measured from the position associated with maximum expansion space. If the time t is likewise measured from the moment when α is zero, then $\alpha=\omega t$, ω being the angular velocity of the shaft;

φ = the phase difference between the variations in volume of the expansion and compression spaces (φ is positive when V_E leads in phase).

To carry out the calculation it is necessary to establish the variation of the pressure p in the machine as a function of the crank angle α.

Variation of the pressure

The expression for the pressure variations derived previously [1]) simply by applying the gas laws is:

$$p = p_{\max}\frac{1-\delta}{1+\delta\cos(\alpha-\Theta)} \quad . \; . \; . \; (4)$$

where $p_{\max}$ is the maximum pressure,

$$\delta = \frac{\sqrt{\tau^2+w^2+2\tau w\cos\varphi}}{\tau+w+2s},$$

Θ is the phase angle of the pressure with respect to the volume of the expansion cylinder (p is at its minimum when $\alpha=\Theta$); hence

$$\tan\Theta = \frac{w\sin\varphi}{\tau+w\cos\varphi}. \quad . \; . \; . \; . \; . \; (5)$$

Formula (4) applies to both the gas refrigerating machine and the hot-gas engine. The value of the quantity δ, which is only slightly dependent on the temperature ratio, is about the same for machines of both types, i.e. 0.3-0.4. *Accordingly, the pressure variations in both machines are virtually the same; there is, however a consider-*

---

[4]) We draw attention to this fact, because in the article quoted, the transition from engine to refrigerator is effected by reversing the direction of rotation. This is not quite so simple (especially as regards the calculation given below), since the sign of the heat flux changes with the direction, and the two cylinders thus exchange functions.

able difference between the two as regards the phase Θ of the pressure with respect to the piston movement. This is substantiated by expression (5) for tan Θ; the denominator of this formula contains the ratio τ, which in the engine is less than unity and in the refrigerator greater than unity. Thus Θ is greater for the engine than for the refrigerator. This is also demonstrated by *fig. 8*, which is a polar diagram showing p as a function of the crank angle, in accordance with equation (4); the resultant curve is an ellipse, one of whose foci coincides with the origin. Fig. 8*a* applies to a refrigerator, 8*b* to an engine; it will be seen that there is a difference in the position of the major axis, which corresponds to the difference in phase angle Θ.

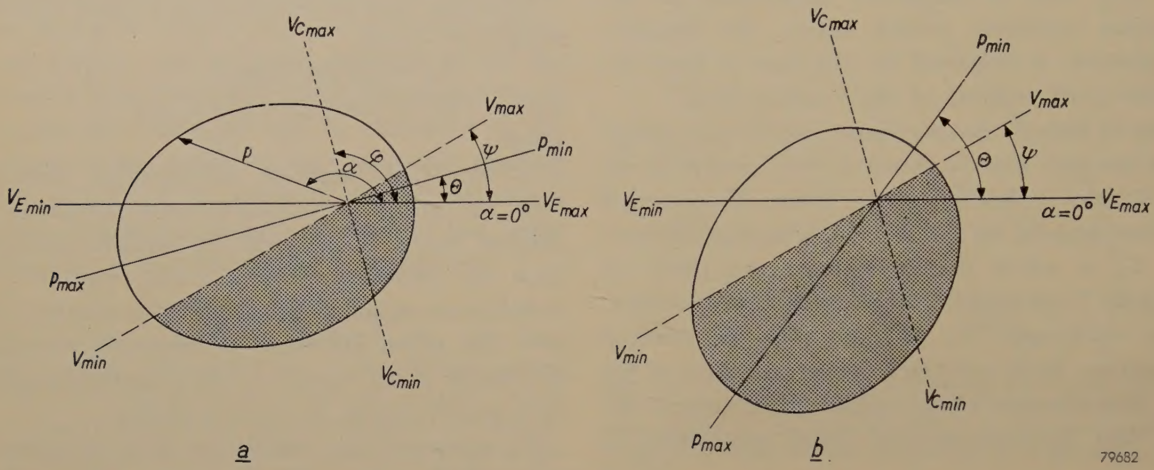

Fig. 8. Polar diagram showing the variation of pressure with the crank angle α,
a) for the gas refrigerating machine ($\tau > 1$),
b) for the hot-gas engine ($\tau < 1$).
Angle α is measured from the position of the crank corresponding to maximum expansion space ($V_E = V_0$). For clarity in the drawing, the pressure ratio $p_{\max}/p_{\min}$ is given a value appreciably higher than the values employed in practice (2 to 2.5). Usually, angle φ is chosen between 60° and 120°. In case (*a*) the phase angle Θ of the pressure variation is smaller than the phase angle ψ of the variation in the total volume $V (= V_E + V_C)$, whereas in case (*b*) Θ exceeds ψ. As a result, the average pressure in the *refrigerator* is lower during the expansion stroke (from $V_{\min}$ to $V_{\max}$, shaded part of ellipse) than during the compression stroke (from $V_{\max}$ to $V_{\min}$); hence mechanical power has to be supplied to the refrigerator. The opposite is the case for an *engine* (*b*): this therefore *delivers* mechanical power.

To further clarify the phase relationship, the pressure p defined by equation (4), the volumes V_E and V_C, and the total volume $V_E + V_C = V$ ("working space") of the refrigerator, are shown in *fig. 9* as functions of α on cartesian co-ordinates. It is seen that the pressure variation is almost sinusoidal.

The minimum and maximum pressures occur at $\alpha - \Theta = 0$ and $\alpha - \Theta = \pi$ respectively. Substitution in (4) gives us for the pressure ratio:

$$\frac{p_{\max}}{p_{\min}} = \frac{1+\delta}{1-\delta} \quad . \; . \; . \; . \; . \; . \quad (6a)$$

By integrating the pressure with respect to the crank angle α, we find an expression for the mean pressure:

$$\bar{p} = p_{\max}\sqrt{\frac{1-\delta}{1+\delta}}, \quad . \; . \; . \; . \quad (6b)$$

which will be used in the calculation that follows.

Refrigerating capacity, shaft power and efficiency

Consider now, quite generally, a working fluid in an enclosed space. The quantity of heat absorbed by this fluid when volume (V) and pressure (p) both vary *sinusoidally* can be determined very simply.

This quantity is, per cycle,

$$Q = \oint p\,\mathrm{d}V. \quad . \; . \; . \; . \; . \; . \; . \; . \; . \quad (7)$$

Now, suppose that

$$V = \tfrac{1}{2}V_0(1+\cos\alpha)$$

and

$$p = \bar{p}\,[1 - \Delta\cos(\alpha - \vartheta)], \quad . \; . \; . \quad (8)$$

where ϑ is the phase lag of the pressure relative to the volume. Substituting the above in (7) we have:

$$Q = \tfrac{1}{2}\bar{p}V_0 \oint [1 - \Delta\cos(\alpha-\vartheta)]\sin\alpha\,\mathrm{d}\alpha,$$

i.e.

$$Q = \pi\bar{p}V_0\frac{\Delta}{2}\cdot\sin\vartheta \quad . \; . \; . \; . \; . \quad (9)$$

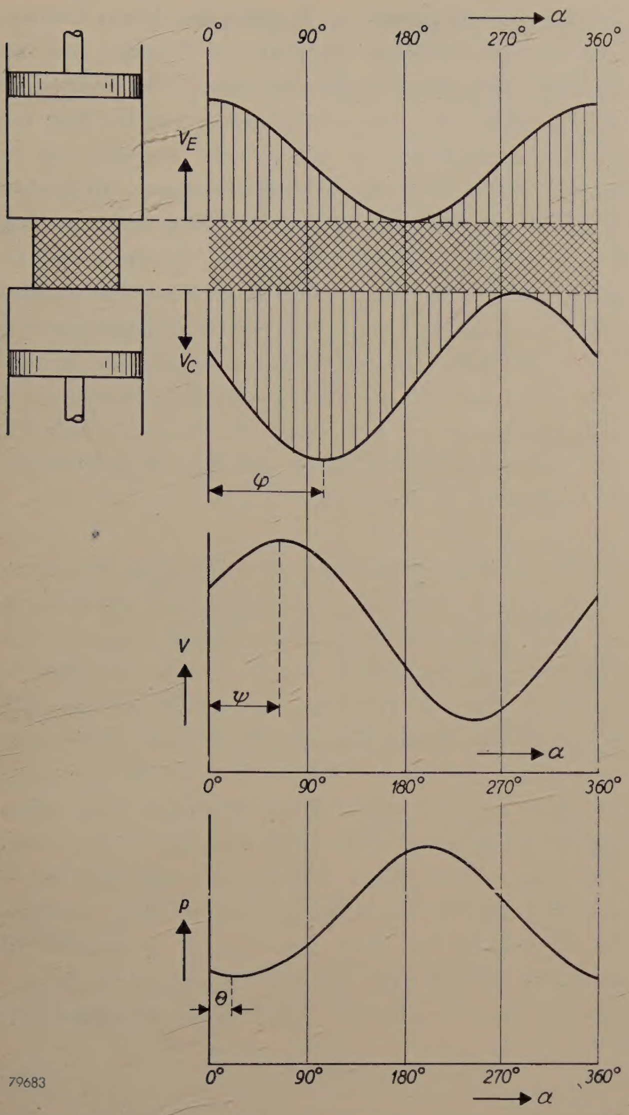

Fig. 9. The variation of the volumes V_E and V_C, of the total volume V ("working space"), and of the pressure p of the refrigerating machine as functions of the crank angle α. The phase relationships are clearly seen; the pressure variation is almost sinusoidal.

It will be seen that Q is positive when angle ϑ is positive, and negative when this angle is negative. This is actually the case in the machine: the pressure lags behind the volume of the expansion space (where the working fluid absorbs heat), whereas it leads the volume of the compression space (where the working fluid liberates heat).

To apply (7) to the cylinders of the gas refrigerating machine, it is necessary to substitute the sinusoidally varying volumes V_E and V_C according to (3), and the non-sinusoidally varying pressure according to (4) [5]. As is well-known, only the fundamental component of (4) will contribute to the integral of the product of (3) and (4). Hence we again obtain (9) in which, as the Fourier series shows, $2\delta/(1+\sqrt{1-\delta^2})$ must be substituted for Δ, and $\vartheta = \Theta$ must be employed for the expansion space and $\vartheta = (\Theta - \varphi)$ for the compression space. We then find the heat absorption per cycle in the expansion space to be:

$$Q_E = \pi \bar{p} V_0 \frac{\delta}{1+\sqrt{1-\delta^2}} \sin\Theta \quad . \quad . \quad (10)$$

and that in the compression space:

$$Q_C = \pi \bar{p}\, w V_0 \frac{\delta}{1+\sqrt{1-\delta^2}} \sin(\Theta-\varphi) . \quad . \quad (11)$$

Using (5), which relates Θ, φ and τ, we deduce from (10) and (11) that:

$$Q_C = -\tau Q_E . \quad . \quad . \quad . \quad . \quad . \quad . \quad (12)$$

The output of cold per second (q_E) is given by multiplying Q_E by the number of revolutions per second. Measuring $\bar{p}$ in kg/cm², V_0 in cm³ and the speed of rotation n in r.p.m., we find [6] that:

$$q_E = 5.136\, \bar{p} V_0 \frac{\delta}{1+\sqrt{1-\delta^2}} \sin\Theta \cdot \frac{n}{1000} \text{ watt.} \quad (13)$$

By analogy with (12), we have $q_C = -\tau q_E$. The power P to be applied to the shaft follows from this and from the equation $P = -q_E - q_C$:

$$P = (\tau - 1)\, q_E . \quad . \quad . \quad . \quad . \quad . \quad (14)$$

Hence the coefficient of performance of the refrigerator is

$$\eta = \frac{q_E}{P} = \frac{1}{\tau-1} = \frac{T_E}{T_C - T_E} \quad . \quad . \quad (15)$$

This is again the thermal efficiency of the Carnot cycle as already derived in the case of the schematic Stirling process and which was to be expected, since the change to a harmonic piston movement does not affect the reversibility of the cycle.

The refrigerating capacity q_E and the shaft power P given by equation (13) and (14) are shown in *fig. 10* as functions of the temperature T_E of the expansion space, when $T_C = 300$ °K (ambient temperature). This diagram demonstrates once again the close relationship between the hot-gas engine and the gas refrigerating machine. Formulae

---

[5] That the expression $Q = \oint p\, dV$, which applies to an enclosed space, is also valid in this case can be demonstrated by means of a thermodynamic argument which has been omitted from this article as being too involved.

[6] On the continent of Europe, refrigerating capacity is generally expressed in kcal/hour: this necessitates changing the constant 5.136 in formula (13) to 4.418. In England and America the units generally used are Btu/hour; in this case the constant in (13) should be 17.7. The watt, however, is a very convenient unit for the calculation of efficiencies, since the power of electric motors is usually expressed in watts.

(12) and (14) apply to both these machines, the difference being that for the hot-gas engine $\tau = T_C/T_E < 1$ and for the refrigerator $\tau > 1$ (hence the phase angles Θ differ in the two cases; see above).

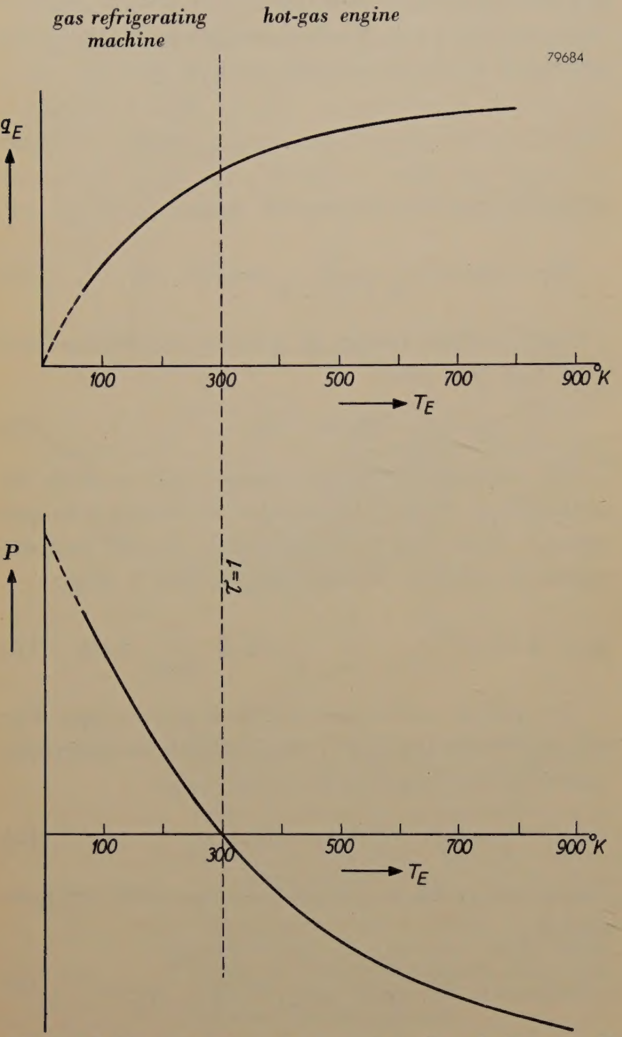

Fig. 10. Refrigerating capacity q_E and applied shaft power P as functions of the temperature T_E of the expansion space (for $T_C = 300$ °K). One continuous curve is obtained, which applies to both the hot-gas engine ($\tau < 1$, to the right of T_C) and the gas refrigerating machine ($\tau > 1$, to the left of T_C).

It is seen that a decrease in T_E is accompanied by a continuous decrease in q_E, and that the passing of the ambient temperature takes place without any discontinuity. Similarly, the variation of the applied shaft power P is continuous, but changes sign when the expansion cylinder drops below ambient temperature; when this happens the machine changes from a hot-gas engine into a refrigerator.

Fig. 10 illustrates the fact, deduced earlier from considerations of the schematic process, that the efficiency decreases rapidly as the freezing-temperature T_E decreases. This happens because the output of cold diminishes and the required shaft power increases as T_E becomes lower (naturally, a high ambient temperature T_C also has an unfavourable effect on the efficiency). *For economical refrigeration, then, it is essential to ensure that the freezing-temperature at which the machine is to operate* is *not lower than strictly necessary.* Incidentally, this conclusion is valid for every refrigerating process. For example, it is most uneconomical to store cold in the form of liquid air when the objects need be cooled only to —100 °C. This demonstrates the importance of a refrigerator capable of operating economically within the virtually unexploited temperature range between —80 °C and —180 °C. The Philips gas refrigerating machine is particularly well adapted to this role.

This article treats only the *ideal* gas refrigeration process. Naturally, the practical application of this process will involve certain losses. The factors governing these losses will be studied in detail in the second article. It will be shown that although the losses are not to be underestimated, it is none the less possible to design a refrigerating machine of this type which combines high refrigerating capacity with small dimensions and high efficiency. This claim will be substantiated by a detailed description of the gas refrigerating machine illustrated in fig. 2 in this article. A number of machines of this type are now in regular use in the Philips factories for the production of liquid air.

Summary. Although the possibility of generating cold by "reversing" the hot-air engine has been known for more than a century, previous attempts to usefully apply the gas refrigeration cycle have been unsuccessful. The application of principles analogous to those of the Philips hot-gas engine has made possible the construction of a highly satisfactory gas refrigerating machine. A number of machines of this type which cool down to about —200 °C, are at present in regular use in the Philips factory at Eindhoven, where they are used for the liquefaction of air: this low temperature is reached in one stage, which makes for a refrigerator of small dimensions and high efficiency. The gas refrigerating machine is, however, also very suitable for operation throughout the entire range of temperatures between —80 °C and —200 °C, which is just the range not covered by refrigerators of conventional design. In this article, the gas refrigeration cycle is described and analyzed with reference to a schematic cycle involving a discontinuous movement of two pistons in two cylinders. It is demonstrated that this schematic cycle can be replaced by a practical cycle based on a harmonic piston movement. The close relationship between this cycle and that of the hot-gas engine is explained in detail. Finally, the pressure variation for an ideal gas refrigeration cycle (no losses) involving a harmonic piston movement, is deduced by applying the previously derived theory of the hot-gas engine. The refrigerating capacity, required shaft power and coefficient of performance (efficiency) are computed from the pressure variation.

In a subsequent article the losses involved in the practical application of this process will be analyzed, and the construction of a complete refrigerating machine described.

A NEW AUTOMATIC HYSTERESIS CURVE RECORDER

by F. G. BROCKMAN *) and W. G. STENECK *).

621.317.44.087.4

In the development of new magnetic materials, the taking of hysteresis curves is one of the recurring measurements. For this purpose an apparatus has been developed which traces a complete hysteresis loop on paper in about a minute. The scales along both axes of this graph can be set at convenient values. According to requirements either the induction or the magnetization may be plotted against the field strength.

Introduction

Measurement of magnetic quantities by integration

The various curves which relate the magnetic induction B (or alternatively the magnetization J), to the field strength H, in ferromagnetic materials (hysteresis loops, initial magnetization curves, minor loops) contain data of practical as well as of theoretical value. Determinations of these data are therefore of considerable importance. More often than not, the determination of at least one, and frequently of both quantities B and H is accomplished by measuring the electromotive force produced in a coil of wire by a change in the magnetic flux. This electromotive force, e, expressed in volts, obeys the relationship:

$$e = \frac{\mathrm{d}N\Phi}{\mathrm{d}t}$$

where Φ is the flux in webers (Vsec) linked by each of the N turns of the coil. In order that the electrical effect can furnish a measure of the flux change producing it, an integration of the voltage developed must be performed:

$$\int_0^t e\,\mathrm{d}t = \Delta N\Phi \quad . \; . \; . \; . \; . \; . \; . \quad (1)$$

Let us suppose, in order to consider a definite case, that the hysteresis curve of a permanent magnet material is required. The sample, which is in the form of a cylinder, is clamped between the pole pieces of an electromagnet (*fig. 1*). A number of windings are laid closely around the sample, constituting a coil for the measurement of B. A small coil, having many turns, is placed adjacent to and with its axis parallel to the sample. This serves to measure H, the value of which, at the site of this small coil, may be taken as equal to the value inside the sample. (Alternatively, and more exactly, a Rogowski or Chattock potentiometer coil may be used to measure H).

Each measuring coil is connected to an integrating device. Such a device may take a number of forms, the most widely known of which is probably the ballistic galvanometer. The ballistic galvanometer is a single deflection device (returning to zero after each reading of a change in flux). Consequently, point by point readings of flux changes must be made, which make the procedure very time-consuming. An advantage of the method is its high accuracy.

Other methods of carrying out the integration make use of the fact that the current through an inductor is proportional to the time integral of the voltage drop across it, or that the voltage developed across a capacitor is proportional to the time integral of the current flowing into it.

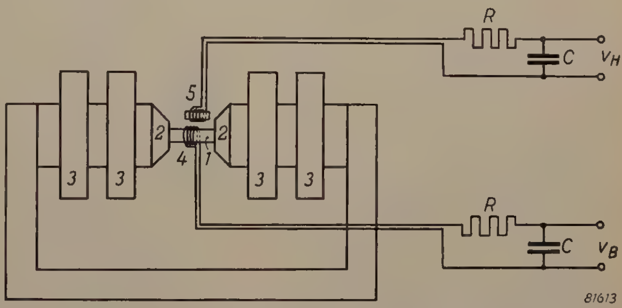

Fig. 1. Principle of hysteresis curve plotting by the yoke method The sample *1* is clamped between the polepieces *2* of the soft iron yoke with magnetizing coils *3*. A coil *4* of a few turns, laid closely round the sample, serves for the measurement of B, and a small coil *5* of many turns for the measurement of H. Both measuring coils are connected to an RC integrating circuit. The voltages v_B and v_H across the capacitors measure changes of the induction and of the field strength in the sample.

Integration with an RC-circuit

The method actually used here is based on the last mentioned principle. Let us for a moment suppose that each of the measuring coils in fig. 1 is connected to a capacitor C via a resistor. If the total resistance in such a circuit is R, the current i and the electromotive force generated in the coil by a changing flux e, the voltage across C being denoted by v, there exists the relation:

$$e = iR + v\,.$$

---

*) Philips Laboratories, Irvington, N. Y., U. S. A.

By combining this with (1) and supposing that we start with an uncharged capacitor, one easily deduces:

$$\Delta N\Phi = RCv + \int_0^t v\,\mathrm{d}t. \quad . \quad . \quad . \quad . \quad (2)$$

It can be arranged that the last term is small compared with the error allowed in the determination of the flux change. In that case we may neglect this term and consider the voltage across the capacitor as a measure for the flux change that has occurred since the start of the experiment.

As the cross-section A_B of the permanent magnet sample and the number of turns N_B around it are known, it is now possible to compute the change in the value of B from the voltage v_B across the corresponding capacitor with the formula:

$$\Delta B = \frac{RC}{N_B A_B} v_B. \quad . \quad . \quad . \quad . \quad . \quad (3)$$

By a similar procedure we may calculate the value of the change in field strength ΔH from the voltage across the capacitor associated with the field-coil. The effective turns-area ($N_H A_H$) of this coil must first be determined by calibrating it in a known magnetic field. When the magnetizing current of the electromagnet is varied, each pair of instantaneous values v_B and v_H provides a point of the required hysteresis curve.

The error on integration

A fuller analysis, not reproduced here, shows that if the magnetic flux is any given function of time, the value of the neglected error term in (2) decreases relative to the main term RCv as the time constant $\tau = RC$ of the integrating network increases. It further appears that in practical cases this error term may be neglected when τ is long compared with the time for the integration. Obviously, however, when the value of τ is increased by increasing R, C, or both, the value of the voltage v itself is decreased, which implies a loss in *sensitivity*. On account of this, and also because it is difficult to obtain large-valued resistors and capacitors that are sufficiently stable, the simple RC integrating circuit turns out to be practicable only for relatively short integration times (e.g. 1/50 second).

RC-integrating circuits, such as outlined above, have been applied to the recording of magnetization curves under alternating current conditions. In the case of the permanent magnet sample we are considering here, rather intense magnetizing fields are required. It is not practicable to produce these fields at A.C. mains frequencies because of the great inductive reactance of the electromagnet and the large eddy currents that would be set up in its unlaminated core. Moreover the eddy currents present in a massive metallic sample would impair the accuracy of the measurements by their shielding effect in the sample. Carrying a laboratory electromagnet of modest size through a cycle from zero field to a large positive field, through zero again to an equally large negative field and back to zero,

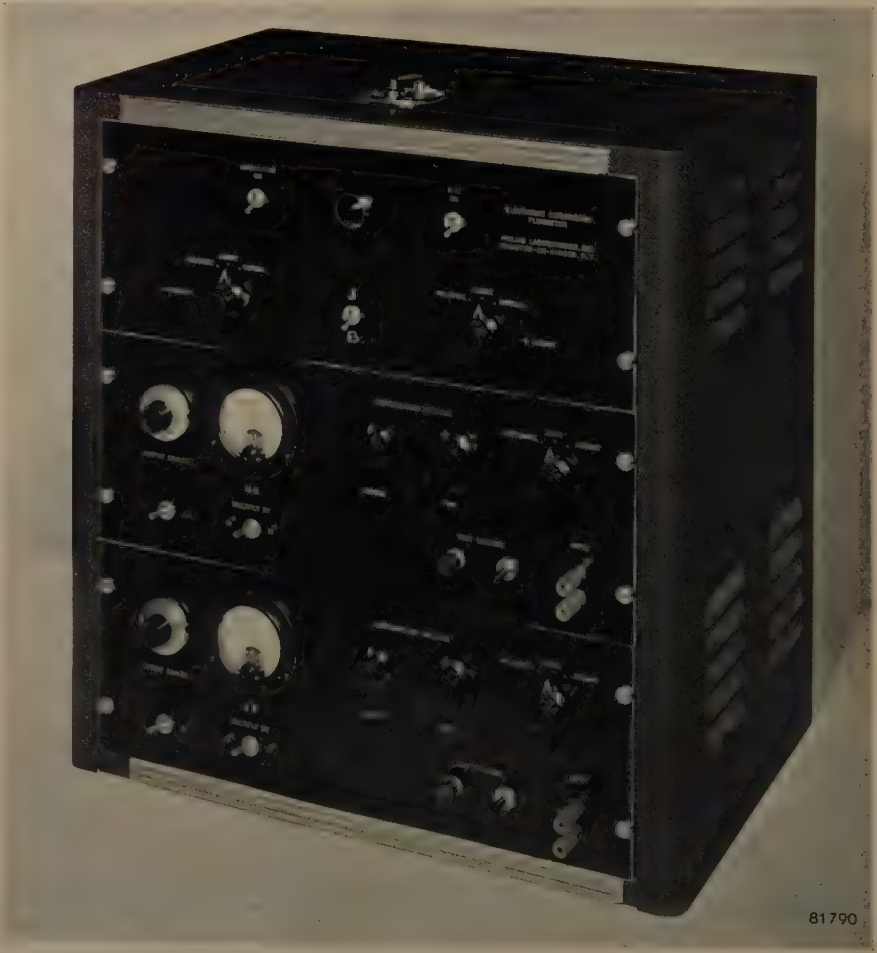

Fig. 2. Front of the instrument for the automatic recording of hysteresis curves, showing two integrator panels (one for B and one for H) and the output control panel (the uppermost one). The instrument is used together with an X-Y recorder of a commercial type.

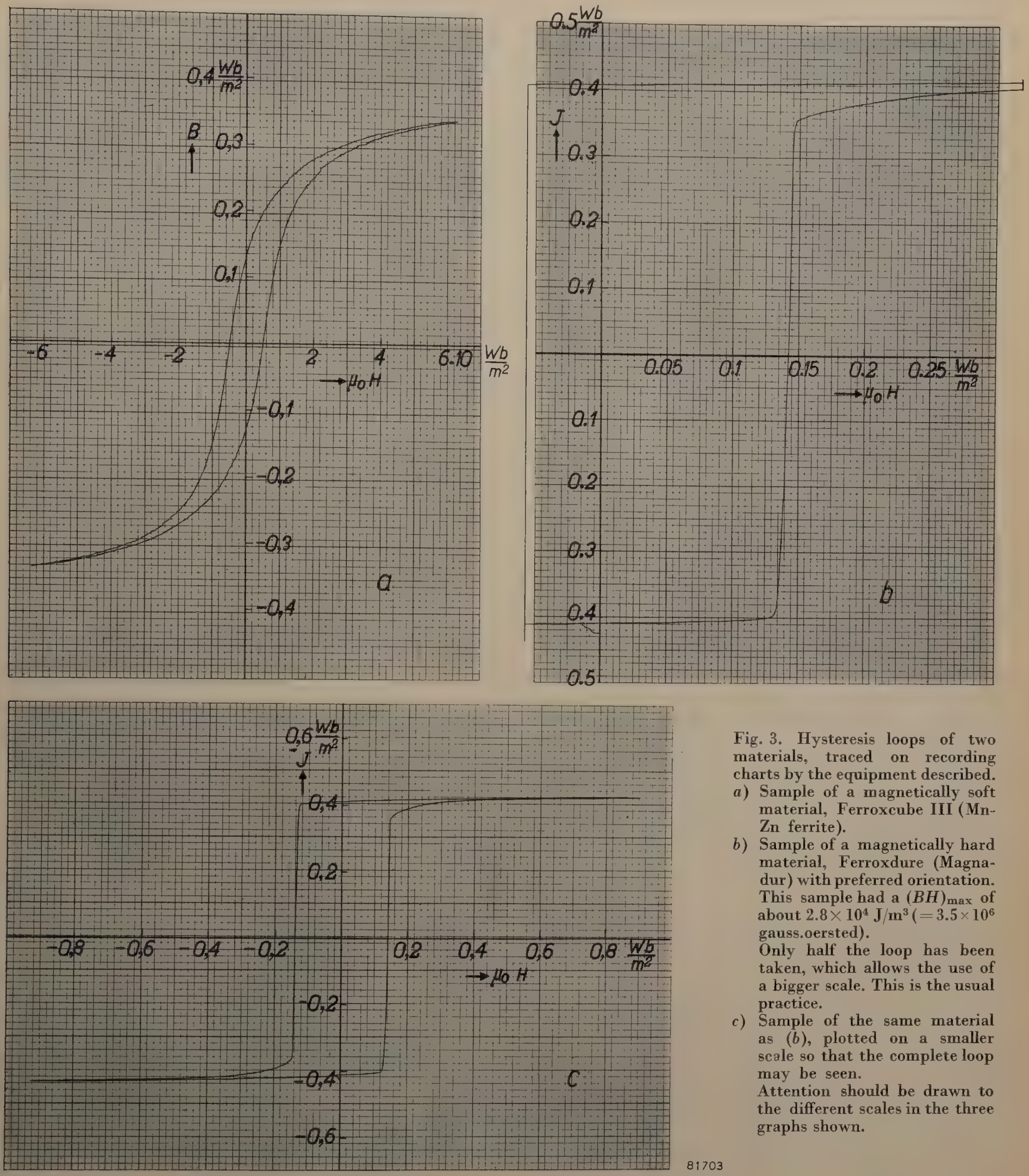

Fig. 3. Hysteresis loops of two materials, traced on recording charts by the equipment described.

a) Sample of a magnetically soft material, Ferroxcube III (Mn-Zn ferrite).

b) Sample of a magnetically hard material, Ferroxdure (Magnadur) with preferred orientation. This sample had a $(BH)_{\max}$ of about 2.8×10^4 J/m³ ($= 3.5 \times 10^6$ gauss.oersted).
Only half the loop has been taken, which allows the use of a bigger scale. This is the usual practice.

c) Sample of the same material as (*b*), plotted on a smaller scale so that the complete loop may be seen.
Attention should be drawn to the different scales in the three graphs shown.

would require perhaps one or two minutes. Obviously the *RC*-integrating circuits would fail under these circumstances.

The new equipment for the recording of hysteresis curves

The instrument which is the subject of this article, and which was developed at the Philips Laboratories at Irvington, N.Y., U.S.A., comprises two identical integrating units and an output control panel (*fig. 2*). The integrating units are refinements of the *RC*-circuits discussed above. They make possible the use of the relatively long integration times necessary with permanent magnet materials. The integrators are calibrated as fluxmeters to an accuracy of about 0.1 %. The unit measuring B and that measuring H are used to move the writing pen and the paper respectively of an X-Y recorder. When the sample is cycled by varying the magnetization current of the electromagnet in a suitable way, the hysteresis curve of the sample is then automatically recorded. In this way a complete hysteresis-loop can be obtained in one or two minutes (*fig. 3*).

If the Rowland ring method of taking the magnetization data is employed, where the current in the primary winding is used as a measure of the field strength, the voltage drop across a series resistor in the primary can serve directly to operate the *H* coordinate of the recorder. Only one of the integrating units is necessary in this case.

Basic circuit of the integrators

The basic circuit used in the fluxmeters (integrators) is shown in *fig. 4*. In this circuit, where *A* represents a D.C. amplifier of very high gain, the principle of negative feedback has been used to increase the time available for the integration ¹).

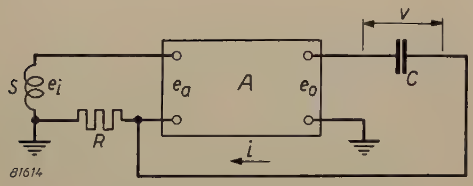

Fig. 4. Basic circuit of the integrators.

For simplicity, let us suppose that the gain *G* of the amplifier is infinite. Then the input voltage e_a of the amplifier must always be zero and consequently the same applies to the current through the search coil S. The voltage e_i generated in the search coil, will therefore be equal and opposite to the voltage drop across *R* developed by the output current *i*:

$$e_i = i\,R, \quad . \; . \; . \; . \; . \; . \; . \; . \qquad (4)$$

or, by integration, assuming that we start with an uncharged capacitor:

$$\varDelta N\varPhi = \int_0^t e_i\,\mathrm{d}t = R\int_0^t i\,\mathrm{d}t = RCv. \quad . \qquad (5)$$

It is seen that the voltage *v* across the capacitor is proportional to the change $\varDelta N\varPhi$ in the flux linked by the search coil.

As explained in the appendix, with a *finite* value of *G*, the circuit acts with the same accuracy as would a resistance-capacitance integrator in which the time constant *RC* is multiplied by a factor approximately *G*/3. The loss in sensitivity that would occur in an ordinary *RC* circuit with a large time constant, however, is now completely avoided.

To raise the time constant of a resistance-capacitance combination of convenient value (say $RC = 10^{-3}$ seconds) to a usuable value (say 10^3 seconds), the amplification must accordingly be several millions.

A physical picture of this increase in time constant can be gained in the following manner. Let a charge reside in C, and suppose that there is no e.m.f. in the search coil. Without amplification, the charge flows out of C through R with the usual decay rate associated with the discharge of a capacitor. In the circuit of fig. 4, however, the voltage drop across R gives rise to a voltage across the input of the amplifier, the output of which is fed into the RC network again. Assuming that this output voltage has the correct polarity, it tends to maintain the charge in C. If the gain, G of the amplifier were infinite, the charge in C would remain an infinitely long time.

The amplifier output voltage as a measure of the flux change

Equations (2) and (5) are both valid on the assumption that the charge on the capacitor is equal to the time integral of the current flowing into it. This is true, however, only when the insulation between the capacitor plates is perfect, a condition which is never completely fulfilled. Accordingly equation (2) does not hold exactly and neither does equation (5), not even when *G* is infinite. It is obvious that the error caused by a non-perfect insulation is much more serious in the case where the time for the integration, and consequently the time for the leakage current to flow, is so much longer. Consequently special care has been given to the insulation in the capacitor. Polystyrene is used as the dielectric and the insulation resistance is in excess of 10^{12} ohms. It is difficult to measure in a simple way the voltage across the capacitor without at the same time seriously reducing this very high insulation resistance. This is why, instead of the voltage *v* across the capacitor proper, the output voltage e_o of the amplifier is used as a measure of the flux change.

In the case of infinite *G* there exists between e_0 and *v* the relation (cf. (4) and (5))

$$e_o = v + i\,R = \frac{1}{RC}\int_0^t e_i\,\mathrm{d}t + e_i. \; . \; . \qquad (6)$$

In practical cases, the error made by equating e_o to *v* is negligible (see appendix), and equation (5) may be replaced by:

$$\varDelta N\varPhi = \int_0^t e_i\,\mathrm{d}t = RCe_o, \; . \; . \; . \; . \qquad (7)$$

---

¹) This circuit using capacitive negative feedback is known as the *Miller integrator* and is commonly used for integration in analog computers, but usually the time constants involved are small compared with the values here. Cf. J. M. L. Janssen and L. Ensing, Philips tech. Rev. **12**, 319-335, 1950/51. R. H. Dicke, Rev. sci. Instr. **19**, 533-534, 1948, has described a capacitative feedback integrator with a long time constant. His method of obtaining D.C. amplification differs from the method used here.

and (3) becomes:

$$\Delta B = \frac{RC}{N_B A_B} e_o \, . \quad . \quad . \quad . \quad . \quad . \quad (8)$$

The amplifier

Of the various systems of D.C. amplification it appears that the galvanometer-photoelectric amplifier is the type which has been developed to the state were useful gains of the required order can be realized. This type of amplifier is used in the integrators.

The principle of the photoelectric amplifier may be understood from *fig. 5*. The terminals of the galvanometer *Ga* constitute the input terminals of the amplifier. *F* is a twin phototube whose two photoelectric elements *I* and *II* are connected in series. Suppose that, when no current is flowing through the galvanometer coil, the light spot from the galvanometer illuminates small but equal parts of each of the photosensitive cathodes. The two elements (supposed identical) then offer the same resistance to the photo-current and consequently the potential of *A* is half the potential drop across the whole phototube. When a small voltage is established across the galvanometer, a tiny current flows through its coil and the latter is deflected, in such a way, say, that the cathode of element *I* receives more and the cathode of element *II* less light. The internal resistance of *I* then decreases but that of *II* increases. As a consequence the potential of *A* rises sharply. The device thus acts as a voltage amplifier.

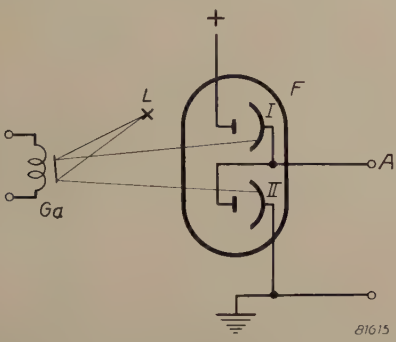

Fig. 5. Illustration of the principle of the photoelectric amplifier

By using a galvanometer of medium-high sensitivity and a working distance of 1 metre, it is possible to obtain an amplifier with a voltage gain of about 50 × 10^6. This amplification is obtained without the use of additional electron tube amplification or positive feedback, and the system thus recommends itself by its obvious simplicity.

Fig. 6 is a simplified circuit diagram of an integrating unit, drawn in such a way as to emphasize its similarity to the basic circuit of fig. 4. A twin phototube *F* of a gas-filled type is used. This gas-filling makes a current limiting resistor necessary in series with the tube. The tube acts as a voltage source with very high internal resistance (> 100 megohms). In order that the output can provide the charging current for the integrating condenser and also operate an indicating instrument, it is necessary to convert this high resistance into one much lower. This is accomplished by a cathode follower vacuum tube circuit.

The meter, shown by $N\Phi$ in the diagram, corresponds to the meters visible in fig. 2. It measures the output voltage of the amplifier and is calibrated directly in units of flux, thus giving a direct reading of changes in the flux linked by the search coil.

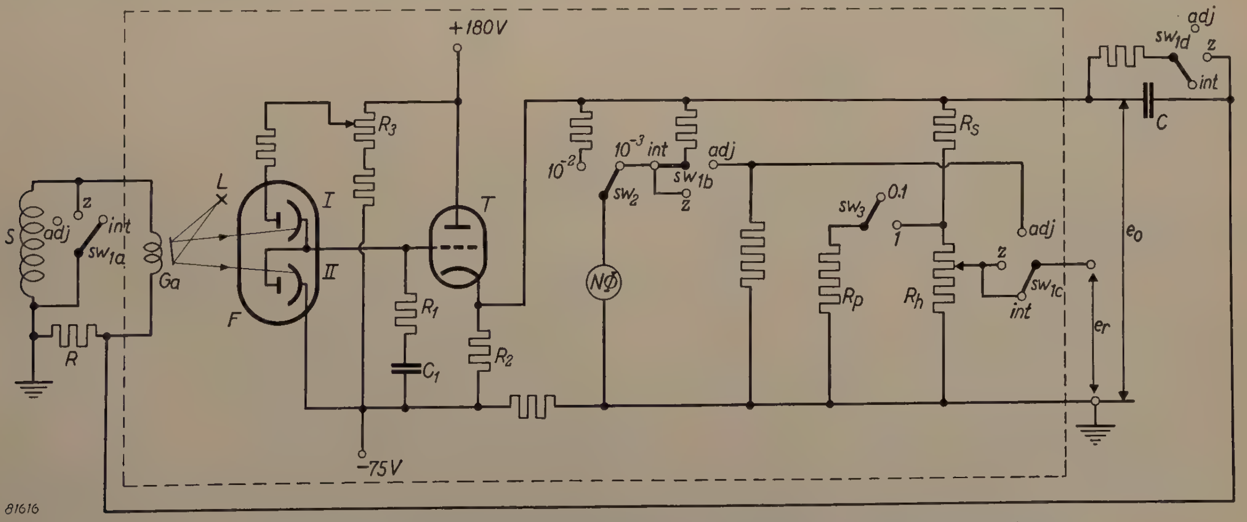

Fig. 6. Simplified diagram of an integrating unit. *S* search coil; *R* integrating resistor; *Ga* galvanometer; *L* light source for galvanometer; *F* gas-filled twin phototube, containing the two photoelectric elements *I* and *II*; *T* cathode follower tube; $N\Phi$ meter giving a direct reading of the change of flux linked by the search coil. By means of the switch sw_2 this meter can be set to two ranges. R_2 ten turn helical potentiometer, serving as an "output scaler"; R_s and R_p resistors in series and parallel to R_h, serving for the adjustment of the output scaler; sw_3 switch to select the range of the output scaler; *C* integrating capacitors; sw_1 (*a*, *b*, *c* and *d*) multiple switch, which can be set to the "integrating position" (int), to zero (z) and to the "adjusting position" (adj.).

With equal light distribution on the two photocells, it is required that the $N\Phi$ meter indicates zero, which implies that the voltage drop across R_2 has to be 75 volts. In the initial setting-up of the equipment, this requirement is met by adjusting R_3 for zero output voltage when the light beam is equally divided on the photocells. The cathode follower circuit is designed so that under these initial conditions tube T operates linearly.

The resistor R_1 and the capacitor C_1, which connect the grid of T to the -75 V line, serve to provide adequate damping of the system.

The measuring range

With the chosen values of R and C ($R = 1000$ ohms, $C = 10^{-6}$ farad) it follows from equation (7) that

$$N\Phi = 10^{-3}\, e_o.$$

With the small receiving type tubes used in the cathode-follower, a maximum value of 10 volts for e_o is easily attainable. This means that flux changes up to 10^{-2} weber can be measured. By means of the switch sw_2 the measuring range of the indicating meter can be set to 10^{-2} weber or 10^{-3} weber.

This is one of the advantages in the use of the capacitance type integrator as compared with the inductance type. Edgar [2]) described a fluxmeter using a mutual inductance. Although he analyzed his circuit in a different manner, it is readily described as a feedback amplifier with a basic circuit as given in *fig. 7*. When the polarity of e_m is in opposition to that of e_i, and the amplification is large, then approximately $e_i = e_m$.

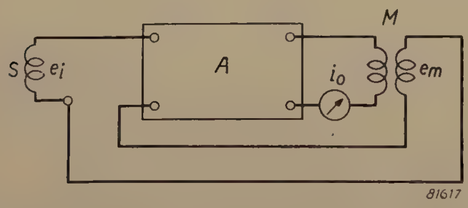

Fig. 7. Basic circuit of the mutual inductance type integrator described by Edgar [2]).

If the input voltage e_i is due to flux changes in a pick-up coil of N turns, then:

$$N\frac{\mathrm{d}\Phi}{\mathrm{d}t} = M\frac{\mathrm{d}i_o}{\mathrm{d}t},$$

where M is the mutual inductance in henries and i_o is the output current flowing in the primary of the mutual inductor. This gives:

$$N\Phi = Mi_o.$$

If the largest practical value of an air-cored mutual inductor (the use of an iron or ferrite cored inductor would impair the accuracy) be 0.1 henry, then to obtain a maximum range of 10^{-2} weber, a change of output current of 0.1 ampère would be required. In vacuum tube circuits, current changes of this magnitude can be obtained only by the use of power tubes. Cioffi [3]) has described an adaptation of the Edgar fluxmeter for use with a pen X-Y recorder.

The output-"scaler"

It is highly desirable that in the recorded curves the scale factors for both coordinates are round figures. Each integrator is therefore provided with an "output scaler", permitting, as explained below, a free choice of these scale factors.

Such an output scaler is in fact a rather simple voltage divider connected across the output terminals of each of the integrators. It consists of a ten turn helical potentiometer R_h in series with a fixed resistance R_s (fig. 6). The recorder is of the self-balancing type (i.e. the input voltage is continuously balanced by an opposing voltage established automatically inside the recorder [4])): the current in its input circuit is therefore zero and its input voltage e_r is exactly proportional to the resistance tapped off. The series resistance R_s is included because in practical cases the output voltages of the integrator are much too large to directly operate the recorder. R_s is so chosen that the voltage e_r at the recorder terminals is variable from 0 to 0.1 of the integrator output voltage e_o. This range can be reduced by means of the switch sw_3 whereby a resistance R_p is connected in parallel with the potentiometer. The value of R_p is such that e_r is now variable from 0 to 0.01 e_o.

The helical potentiometer has effectively 1000 divisions so that, when S is the dial reading, there exists between e_r and e_o the relation:

$$e_r = \frac{S}{1000}\cdot m\cdot e_o\,, \quad . \; . \; . \; . \; . \quad (9)$$

where m is a factor, either 0.1 or 0.01 chosen by the switch.

The X-Y recorder used gives full scale deflections (100 divisions) on both axes at input voltages of 10^{-2} volts (i.e. 10^{-4} volts per division). A deflection of y divisions will accordingly correspond to:

$$e_r = 10^{-4}\, y \text{ volts}\,. \quad . \; . \; . \; . \; . \quad (10)$$

From (8) we find, using (9) and (10);

$$\Delta B = \frac{1}{S}\,\frac{1000\,RC}{m}\,\frac{1}{N_B A_B}\,10^{-4}\,y\,.$$

---

[2]) R. F. Edgar, A new photo-electric hysteresigraph, Trans. Amer. Inst. El. Engrs. **56**, 805-809, 1937.

[3]) P. P. Cioffi, A recording fluxmeter of high accuracy and sensitivity, Rev. sci. Instr. **21**, 624-668, 1950.

[4]) A description of such a system may be found in H. J. Roosdorp, An automatic potentiometer for industrial use, Philips tech. Rev. **15**, 189-198, 1953/54 (No. 7).

The scale factor for the movement connected to the B-integrator is thus

$$1 \text{ division} = \frac{1}{S}\,\frac{1000\,RC}{m}\,\frac{1}{N_B A_B}\,10^{-4} \text{ webers/m}^2. \quad (11)$$

R and C are known, and so is the quantity $N_B A_B$, though this value may differ for different experiments. It is seen from (11) that the dial reading S of the potentiometers can be adjusted to give the scale factor along the B-axis a convenient value. The setting of the scale along the H-axis is accomplished in an analogous way.

If we want full scale deflection (100 divisions) to correspond to a value ΔB_1 say, of the change in the induction, 1 division must correspond to $\Delta B_1/100$ webers/m². From (11) it then follows that the dial of the potentiometer should be set to:

$$S = \frac{1}{N_B A_B \Delta B_1}\,\frac{10\,RC}{m} \quad . \ . \ . \ . \ . \ . \ . \quad (12)$$

If R and C had exactly their nominal values of 10^3 ohms and 10^{-6} farads respectively, $10\,RC/m$ would be either 10^{-1} or 1, depending on the position of the switch sw_3. Now R is made equal to its nominal value to an accuracy of 0.1%, but C only to 0.5%. This precision is adequate for the indicating meter $N\Phi$. A closer accuracy, however, is desirable at the recorder. A measurement of C is therefore made to an accuracy of 0.1% (and as a check the same is done for R). In order not to complicate the calculation of the required potentiometer dial setting, R_s and R_p are readjusted to make m deviate from 0.1 or 0.01, as the case may be, to correct for the deviation of the RC product. In this manner $10\,RC/m$ is made equal to 10^{-1} or 1 respectively to an accuracy of about 0.1%. As the helical potentiometer also is accurate to 0.1%, the same order of accuracy is obtained in the voltages applied to the recorder. A commercially available recorder accurate to 0.1% is used and the cumulative errors (see also appendix) then allow a normal accuracy in the recorded curves of about 0.5% of the maximum reading.

Influence of thermo-electric voltages

The input circuit of an integrator unit involves the galvanometer, the search coil and the resistor R. Much care has been taken to reduce the possibility of the generation of thermal e.m.fs in this loop. The precautions include the use of all copper conductors, massive copper terminals and the inclusion of the resistor R (the only non-copper conductor in the circuit) in a thick walled aluminium box. This last measure serves to keep both ends of R at the same temperature. Even with these precautions a means of balancing the last traces of thermal e.m.fs is required; this balancing is done by a network (not shown in fig. 6) which makes it possible to insert a small controllable and reversible current through R. The voltage drop in R can be set to oppose any thermal forces in the amplifier input circuit.

An impression of the necessity for such a control can be gained by the following: when the fluxmeter is set to the highest sensitivity and is used with a recorder giving full scale deflection for 10 mV, a constant input voltage at the integrator of 10^{-7} V will cause the recorder to deflect 10% of full scale in 100 seconds.

Thermal e.m.fs are a real source of trouble in any flux measuring system. In addition to true thermo-electric forces, there is another effect which might be called an "effective" thermal e.m.f. With the precautions taken to eliminate true e.m.fs this "effective" e.m.f. can be observed. It is the shift of the mechanical zero of the galvanometer with temperature. A shift of the mechanical zero has the same effect as a current flowing in the galvanometer coil and therefore as an e.m.f. in the input circuit. Shielding of the galvanometers from temperature fluctuations aids in keeping this effect at a minimum.

The multiple switch sw_1 (a, b, c, d) serves three purposes. In the centre position, the integrating capacitor C is shorted through a high resistance. This resets the fluxmeter to zero output voltage. By switching to the "integrate " position the unit is ready to act as a fluxmeter. The third switch position is used to adjust the thermal e.m.f. balancing current. In this position the unit is also in "integrate" condition, but the sensitivity at the recorder terminals is twice as great as in the most sensitive operating condition. Drift compensation is made under this enhanced sensitivity.

Recording the magnetization

Since the magnetization is given by $J = B - \mu_0 H$, and the two voltage outputs to the recorder are directly proportional to B and $\mu_0 H$, these may be subtracted electrically to give J. The one requirement is that the output scalers of the two units must be set so that the factors relating their output voltages to B and $\mu_0 H$ respectively, are the same.

This requirement is a disadvantage, because it prevents us from choosing the most convenient full scale deflections for both movements of the recorder. The magnetization can, however, be recorded by a somewhat different method, whereby this disadvantage is avoided. This method comes down to the performance of the necessary subtraction on the input rather than on the output side of the integrators. If the effective turns-area products of the B and the H coil were the same ($N_B A_B = N_H A_H$), the desired effect could be obtained by simply subtracting the voltage generated in the H coil from that generated in the B coil, and feeding the resultant voltage into the B (now changed to J) integrator. In practice, the voltage generated in the H coil must first be reduced to the effective turns-area product $N_B A_B$ of the B coil, which means that only a fraction $N_B A_B / N_H A_H$ of this voltage must be subtracted. The required fraction is obtained by the insertion of a voltage dividing potentiometer across the terminals of the H coil. (*fig. 8*) It is one of the advantages of the large amplification of the feedback amplifier that its effective input resistance is so large that use can be made of a potentiometer of a relativvely low resistance, accurate potentiometers of very high resistance not being available. In this case a 1000 ohm potentiometer is used. If the electrical resistance of the H coil exceeds 1 ohm, this must be taken into account in the adjustment of the potentiometer, if an accuracy of 0.1% in the voltage division is to be maintained.

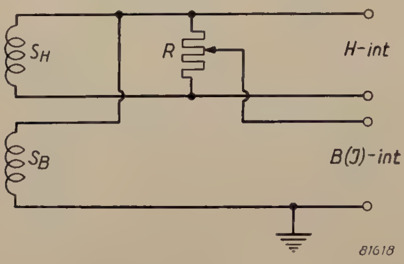

Fig. 8. Input-system for the integrators, suitable for the recording of the magnetization J as a function of the field strength. Correction for the wire size of the B coil can also be made with this circuit. S_H search coil for the measurement of H; S_B search coil for the measurement of B or J; R potentiometer.

It is necessary that the B coil is so wound that its effective turns-area product is less than that of the H coil. Otherwise a fraction greater than unity of the H coil voltage would have to be tapped off the potentiometer, which is of course impossible.

The potentiometer used is a ten-turn helical potentiometer. These components use dissimilar metals for the resistance wire and for the contacts. As has already been pointed out, thermal e.m.fs. in the input circuit are very undesirable and extra care must therefore be exercised to prevent their occurrence. For this reason the potentiometer is contained within a double thermal enclosure. The inner enclosure is of thick-walled copper and the potentiometer is immersed in oil. In this manner temperature differences in the non-copper portions of the circuit are kept to a minimum.

Correcting for the wire size of the B coil

It follows from theory that the total area enclosed by a turn of wire is that enclosed by its centre line. Thus, even when the B coil is laid in intimate contact with the sample, the flux through the turns is made up of two parts, 1) the flux in the sample and 2) the flux passing between the sample and the centre-line of the wire of the coil. The second contribution causes an error in the observed induction B. This can be automatically corrected when use is made of the potentiometer across the H coil mentioned above. If the active area of the flux in the annulus between the sample and the centre line of the wire, be s, then the effective turns-area product is $N_B{\cdot}s$ (N_B is the number of turns of the B coil). Now in the H coil, an effective turns-area N_HA_H corresponds to the total voltage generated in this coil, so that an effective area of $N_B{\cdot}s$ corresponds to the fraction $N_B{\cdot}s/N_HA_H$ of this voltage. If by means of the potentiometer we subtract this fraction of the H coil voltage from the voltage generated in the B coil, the correction for the wire-size of the B coil is automatically made.

Of course the same correction can be made when the magnetization J is plotted. We then have an effective turns-area of $N_B(A_B + s)$ for the H-flux through the B coil and consequently have to subtract a fraction $N_B(A_B + s)/N_HA_H$ of the voltage generated in the H coil.

Appendix: The influence of finite amplifier gain

Equation (5) in the text was developed under the assumption that the gain G of the amplifier was infinite. The circuit conditions when G is finite are given in this appendix. The input resistance of the amplifier and the resistance of the search coil are also included in this analysis. Fig. 4 is redrawn as *fig. 9*. The circuit equations are:

$$\begin{aligned} e_a &= r_i i_1 \\ e_o &= G\, e_a \\ v &= e_o - Ri_1 - Ri_2 \\ e_i &= (r_s + r_i + R)i_1 + Ri_2 \\ \int_0^t i_2\mathrm{d}t &= C\,v \end{aligned}$$

Of the six variables (e_o, e_a, i_1, i_2, e_i and v) in these five equations, the first four can be eliminated, leaving a relation between e_i and v. This relation may conveniently be written in the form

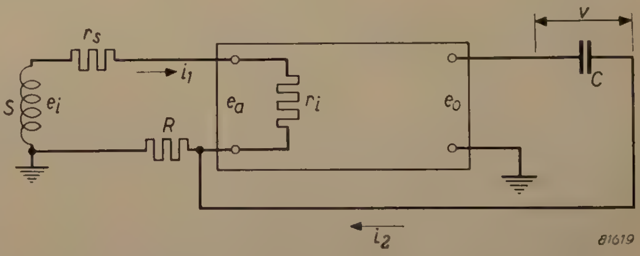

Fig. 9. Basic circuit of integrating unit for the deduction of the circuit equations.

$$\int_0^t e_i\mathrm{d}t = RCv + \frac{r_s + r_i + R}{Gr_i - R}\left[RCV + \int_0^t v\mathrm{d}t\right]. \qquad (13)$$

This result may be compared to the equivalent relation in the case of the simple RC-integrating circuit. There we had:

$$\int_0^t e_i\mathrm{d}t = RCv + \int_0^t v\mathrm{d}t\,. \;.\;.\;.\;.\;.\;.\; \qquad (14)$$

In our case $R = 1000$ ohms and $r_i = 500$ ohms, r_s may be a few ohms and thus its influence is only small. If $G = 50 \times 10^6$, then:

$$\frac{r_s + r_i + R}{G r_i - R} \approx \frac{1}{G/3} = 6 \times 10^{-8}.$$

From this it follows at once that the first correction term in (13) is negligible as compared with the main term. The second correction term is identical to that in (14), except that in (13) it is preceded by a factor of the order 10^{-7}. It follows that the circuit acts as an RC-integrator in which the error on integration is reduced by a factor of about $G/3$ as was stated in the text.

The time constant

If equation (13) is solved for v under the condition that $e_i = 0$, then the decay of the voltage v across the capacitor, when left to itself, can be obtained. This solution shows that v will decay exponentially according to

$$\frac{v(t)}{v(0)} = \exp - \left\{ \frac{1}{RC} \, \frac{r_s + r_i + R}{(G+1) r_i + r_s} \, t \right\}.$$

If the time constant τ is defined as the time required for v to fall to $1/e$ of its initial value,

$$\tau = RC \, \frac{(G+1) r_i + r_r}{r_s + r_i + R}. \quad . \; . \; . \; . \; . \quad (15)$$

With the values mentioned for r_i, r_s, R and G, we find $\tau = \frac{1}{3} G \cdot RC = 17 \times 10^6 \, RC$. Furthermore, since the RC product used is 10^{-3}, the time-constant is about 1.7×10^4 sec $\approx$ 4.7 hours.

The error on integration

In practice not the voltage v across the capacitor, but the output voltage e_o of the amplifier is used as a measure of the time integral of the input voltage e_i. Instead of the relation between v and e_i we can also deduce from the circuit equations a relation between e_o and e_i. Using the expression (15), this relation turns out to be:

$$e_o = \frac{1}{RC} \int_0^t e_i \mathrm{d}t + e_i - \frac{1}{\tau} \int_0^t e_o \mathrm{d}t. \quad . \; . \; . \; . \quad (16)$$

(If G tends to infinity τ does the same and (15) reduces to (6)). Equation (16) shows that the output voltage is not exactly proportional to the time integral of the input voltage, but that two additional terms exist in the solution of the circuit equations. An evaluation of the effect of these terms upon the accuracy of the basic assumption is therefore appropriate. It will not be surprising that certain restrictions exist as regards the time over which the integrations (and hence flux measurements) are made. Although it is not immediately self-evident from (16), a closer comparison of the different terms in this equation shows that the second term on the right ($+e_i$) is associated with a short time limit, and the third term with a long time limit to the integration operation. These two limits are considered separately. In either case it is necessary to define the manner in which the flux in the measuring coil changes in time before an evaluation of these time limits can be made. Both cases have been considered for

a) a flux increasing linearly with time by a fixed amount.

b) a flux increasing according to the square of time by a fixed amount.

c) a flux changing sinusoidally for one cycle, with a fixed maximum value.

The long time limit. — For the analysis of this case, the short time factor in (16) may be ignored and this equation becomes:

$$e_o = \frac{1}{RC} \int_0^t e_i \mathrm{d}t - \frac{1}{\tau} \int_0^t e_o \mathrm{d}t.$$

It is evident that the determining factor in the magnitude of the error term is the time constant τ. If this were infinitely large the error would be zero. It is possible to show that in first approximation the error is proportional to the time used in the measuring operation (the integrating time). With the derived value of $\tau (\approx 280$ min) this approximation is still valid with integrating times of a few minutes. Furthermore, the error will be less than 1% if the integrating time is less than 4 minutes in any of the three flux change functions considered. The sinusoidal variation is perhaps more analogous to the variations experienced in flux measurements. For this case the peak reading is accurate to better than 1% if the time for the cycle is less than 8 minutes.

The short time limit. — When the time of observation is small, then the long time factor term in (16) may be ignored and this equation may be written:

$$e_o = \frac{1}{RC} \int_0^t e_i \mathrm{d}t + e_i.$$

At the end of an integration period, e_i becomes zero and therefore the error is zero.

However, if at any time during an integration, the output voltage at that instant is taken as the instantaneous time integral of the input voltage, this error term exists. Evaluation of the magnitude of this term for the three flux change functions considered shows that the error is less than 0.1% when the time of integration is greater than a few seconds. Because the equipment is used with electro-mechanical recorders with response times of several seconds, this limitation is never important: the operations must in any case be performed so that the changes in the output voltages are slow enough for the mechanical system of the recorder to follow them.

Summary. The equipment described serves for the automatic tracing of hysteresis curves. As usual, B and H are measured by the integration of the electromotive forces which are generated in suitably placed coils when the field is changed. The instrument contains two identical integrators, one for B and one for H, providing output voltages which are the time integrals of their input voltages. These output voltages operate the movements of the paper and the pen, respectively, of a self-balancing X-Y-recorder, so that B is plotted automatically as a function of H. The integrators make use of the fact that the voltage across a capacitor is proportional to the time integral of the current flowing into it. The simple RC integrating circuit, consisting of a capacitor, connected via a resistor to the e.m.f. to be integrated, has the disadvantage that it can only be used when the integration time is short compared with the value of the RC product. For practical reasons the value of this RC product is restricted, so that for integration periods longer than about 1/50 second the simple RC-circuit is not suitable. The integrators actually used avoid this difficulty and may be used for the integration times of one or two minutes which occur in practice when investigating non-laminated samples or samples with high coercivity.

The accuracy of the curves obtained is usually better than 0.5%. The scales along the B and the H axes can be set at convenient values at the beginning of the measurement. It is also possible to obtain directly the magnetization instead of the induction as a function of H. One of the features of the equipment is the employment of an novel input device, making it possible to plot this magnetization, while maintaining free and independent choice of the scales along *both* axes. The same device permits automatic correction for the wire size of the B coil.

A "PHOTOFLUX" FLASH-BULB WITH SIMPLIFIED CAP

by R. WESTRA.

771.448.4

The development of the flash lamp has been especially characterized in recent years by a large increase in the specific light output (i.e. the light output in visual lumen-seconds divided by the bulb volume) and by a reduction in price [1] [2]. A particularly remarkable increase in the specific light output was obtained by the introduction of the "Photoflux" bulb type PF 3, "the smallest flash-bulb in the world", which was put in the market in 1952. This miniature lamp has a maximum diameter of 22 mm and an overall length of 50 mm (*fig. 1c*; in fig. 1*a* and *b* older "Photoflux" lamps have been given for comparison). The PF 3 emits about 5500 lumen-seconds, a quantity of light which is amply sufficient for most amateur purposes. The manufacture of the lamp was made possible by adoption of the manufacturing techniques used for very small incandescent lamps, such as torch bulbs.

Early in 1954 another small flash-bulb made its appearance in America, with a still smaller diameter (20 mm) and a light output which is correspondingly lower (4000 - 5000 lm sec), see fig. 1*d*. Instead of the bayonet lamp cap of 15 mm diameter (BA 15s, see fig. 1*b* and *c*) generally used until then, this lamp has a cap of only 9 mm diameter, provided with a groove by which it is kept in the lampholder. The purpose of the introduction of this smaller and simpler lamp cap was undoubtedly to cheapen its manufacture and to contribute to the popularity of the flash-bulb by way of a correspondingly reduced selling price.

Philips have also gone into the question of further reducing manufacturing costs. In order to analyze the problem and decide which parts merit first consideration with regard to possible simplification, we will enumerate the three main components of which the flash lamp consists:

1) The light-emitting part: a loosely-knit ball of aluminium-magnesium wire of such a length and diameter that on burning in an oxygen atmosphere the wire emits the quantity of light required.
2) The transparent sealed envelope, in the form of a glass bulb which renders the working of the lamp harmless and odourless, and isolates the oxygen filling from the air.

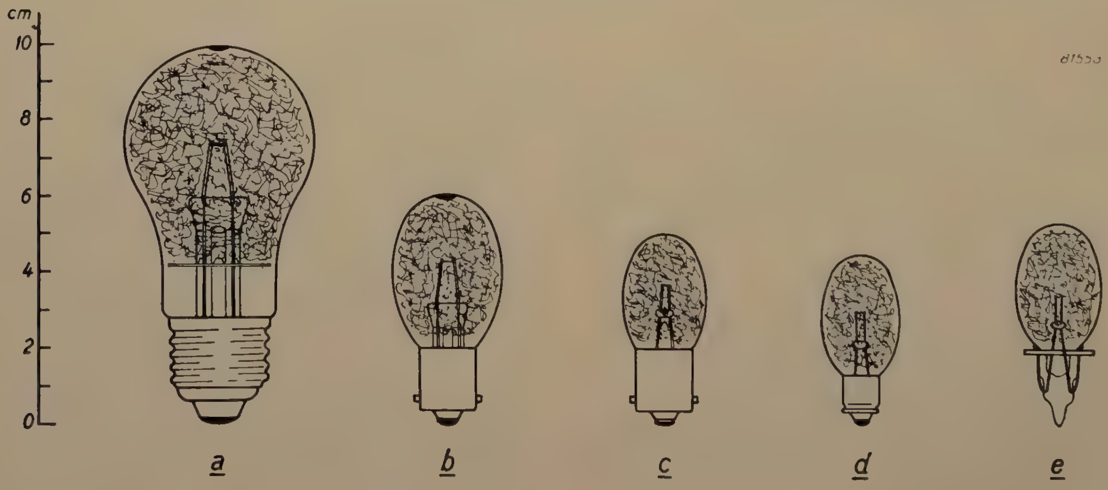

Fig. 1. Different types of flash-bulbs.
a) Lamp in which the lead-in wires for the ignition current are sealed in a "pinch", which also contains the exhaust tube. This construction is now used only for lamps emitting a very great quantity of light, such as the "Photoflux" lamps PF 60 and PF 100.
b) Smaller version of (*a*) with bayonet cap BA 15s. In 1952 Philips replaced this type by the type (*c*). The lamps represented in (*c*), (*d*) and (*e*) are of the "bead-mount" construction (the lead-in wires go through a glass bead).
c) "Photoflux" lamp PF 3 with lamp cap BA 15 s.
d) American flash lamp, with smaller cap.
e) "Photoflux" lamp PF 1, with *glass* cap.

---

[1] G. D. Rieck and L. H. Verbeek, The "Photoflux" series of flash-bulbs, Philips tech. Rev. **12**, 185-192, 1950/51.
[2] L. H. Verbeek, The specific light output of "Photoflux" flash-bulbs, Philips tech. Rev. **15**, 317-321, 1953/54.

3) The electric ignition mechanism: this consists of a paste applied to a tungsten wire which is provided with two lead-in wires; the lead-in wires are soldered outside the bulb to a metal lamp cap which is cemented onto the bulb. When the tungsten wire is brought to incandescence by means of an electric current, the paste ignites and fires the aluminium-magnesium wire.

A considerable saving was realized by mounting the ignition mechanism, not on a "pinch mount" (fig. 1*a* and *b*) but on a "bead mount" (fig. 1*c*), in which the lead-in wires are kept spaced by a glass bead (see the article referred to in footnote [2])). Further saving must be sought, in the first place, in the non-essential parts of the ignition mechanism. The new American construction (fig. 1*d*), with the smaller cap, already shows a tendency in this direction. Philips have looked for an even more radical step however, and the replacement of the metal cap by a (cheaper) glass construction was therefore considered.

This has, indeed, proved possible, by giving the neck of the bulb such a shape that it can take over the two functions of the metal cap, namely to hold the lamp in the reflector and to make contact between the lead-in wires and the ignition current battery. Fig. 1*e* and *fig. 2* show how this has been achieved in the new "Photoflux" lamp, type PF 1.

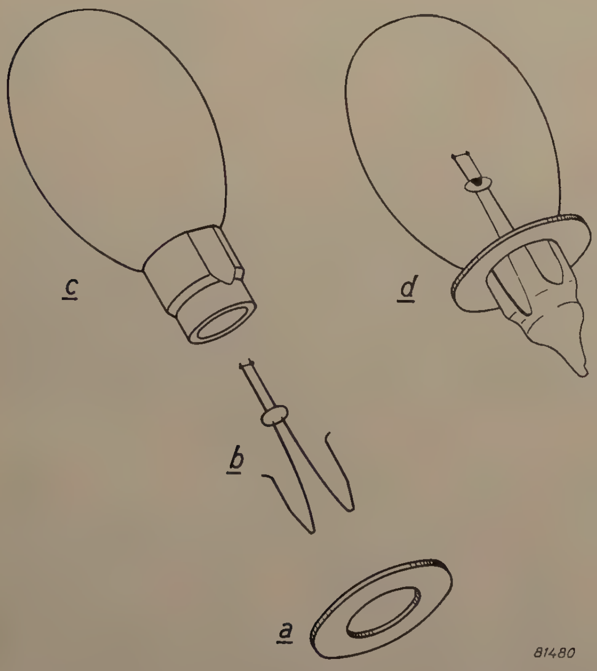

Fig. 2. In the "Photoflux" flash-bulb PF 1, the lead-in wires of the bead mount (*b*) are laid back along the neck of the bulb (*c*), and retained by an insulating ring (*a*). (*d*) The PF 1 complete.

The ends of the lead-in wires outside the bulb are laid back over the neck and are kept tightly in place with a flat ring of insulating material (*a* in fig. 2). The type number of the flash-bulb is marked on this ring. The glass neck is flattened on two sides, so that the lamp is uniquely located in the holder (*fig. 3*), i.e. it can be inserted only in such a way that the lead-in wires make contact with flat springs mounted in the holder. On inserting the lamp, the wires scrape along the springs, thereby ensuring good contact. The springs, moreover, secure the lamp in the holder.

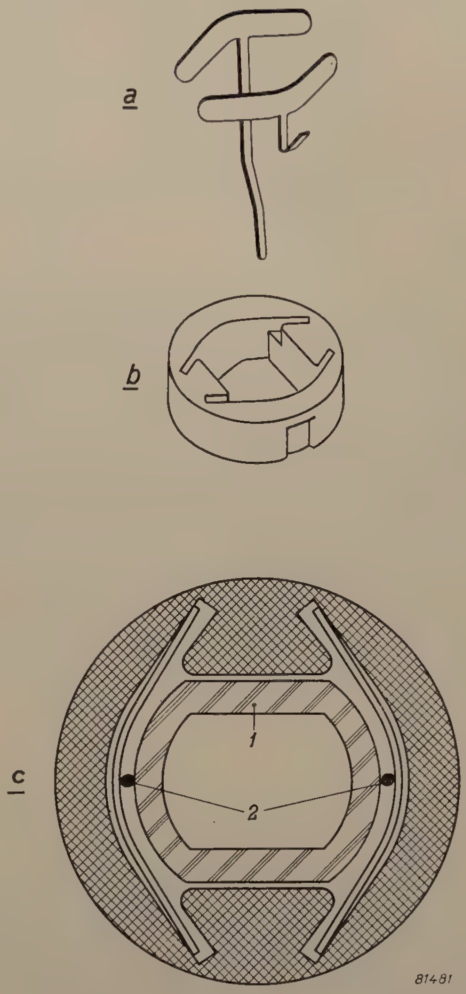

Fig. 3. Lampholder for the "Photoflux" flash-bulb PF 1. *a* flat springs, *b* body of insulating material, *c* holder with lamp inserted (*1* glass neck, *2* current supply wires).

The change in construction described is not at the cost of the luminous output of the flash-bulb: on the contrary the PF 1 has an even greater specific light output than the PF 3.

The introduction of a new fitting necessarily has the drawback that an adaptor must be used until flash equipment is available to take the new design.

The adaptor represented in fig. 3 is small enough to be fitted into a BA 15s bayonet cap (*fig. 4*) for which most flash equipment is at present constructed.

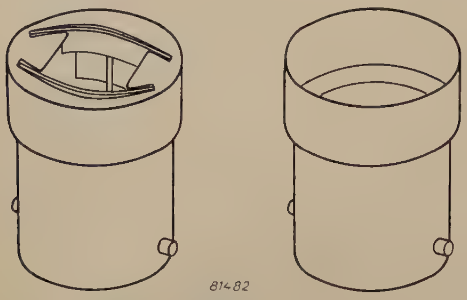

Fig. 4. Left: adaptor, consisting of a BA 15s bayonet cap (right) in which the lampholder of fig. 3 has been placed.

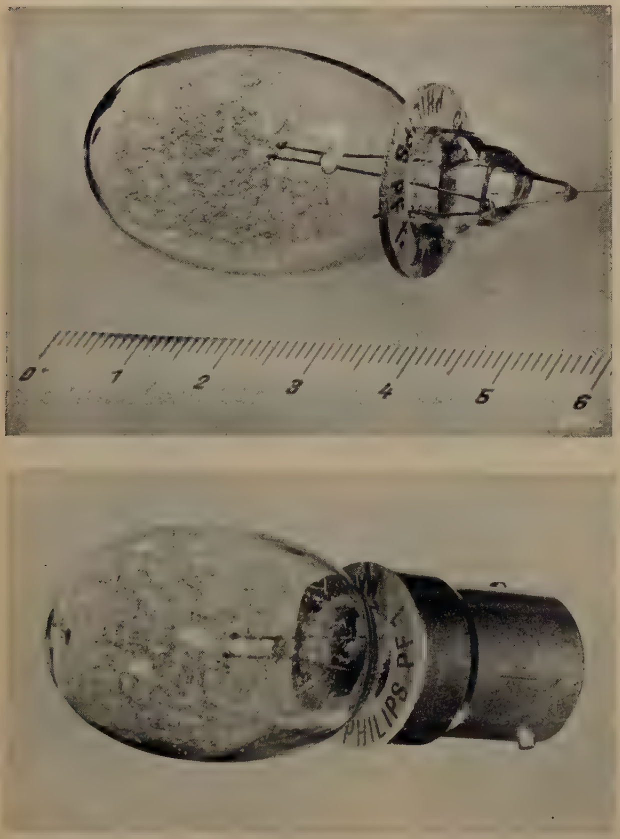

Fig. 5. The "Photoflux" flash-bulb PF 1, with and without adaptor.

Fig. 5 shows the new "Photoflux" lamp, with and without adaptor. The adaptor will of course become superfluous as soon as the makers of flash equipment adapt their lampholders to this latest development in the flash-bulb.

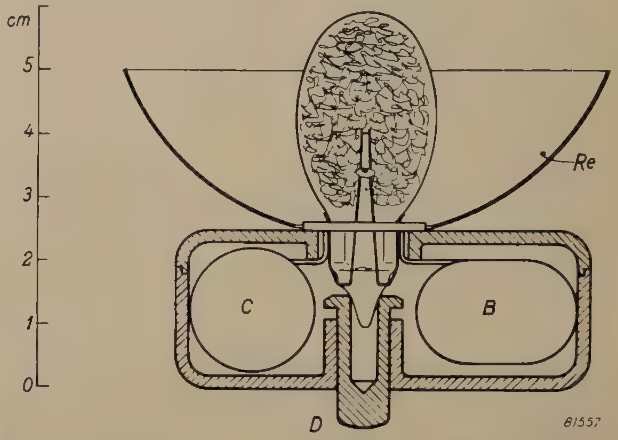

Fig. 6. Flash-bulb equipment with the new "Photoflux" PF 1. The construction of the apparatus shown here is based on ignition with the help of a capacitor (*C*), a method frequently used nowadays. The reflector *Re* has a diameter of 75 mm. *B* is the battery (22.5 V hearing-aid battery). *D* push button for ejecting the used lamp.

In *fig. 6* a section is shown of a flash equipment with the holder for the new flash-bulb. The small dimensions of the lamp also make it possible to use a small reflector, in order to obtain a uniform light distribution. The reflector shown has a diameter of 75 mm. The dimensions of the whole flash apparatus can thus also be made very small, which is of course a further advantage. Used bulbs can be ejected very simply and quickly by means of a push button, thus avoiding the handling of the hot glass envelope.

Summary. A description is given of a "Photoflux" flash-bulb, type PF 1, in which the metal cap used up to now is superseded by the neck of the glass bulb itself; this makes the bulb considerably cheaper. The outer ends of the lead-in wires are bent so that they lie along the neck, and are kept in place by a ring of insulating material. The flash-bulb is secured in the lampholder by the frictional grip of two flat springs, which also serve as connections to the lead-in wires for the ignition current. An adaptor for the new bulb, with a normal BA 15s bayonet cap to fit existing equipment, is described.

THE WEAR OF DIAMOND DIES

by L. SCHULTINK, H. L. SPIER and A. J. van der WAGT.

679.89:549.211:620.178.1

The great value of the diamond is not only due to its rareness and its excellent refractive properties, to which it owes its unique place among precious stones, but equally well to its tremendous mechanical hardness and resistance to wear. These last two properties in particular have won it an unassailable position among materials for tools. Apart from its use for cutting tools, for bearings and as an abrasive, diamond have proved of great value as drawing dies, for producing wire from very hard metals such as tungsten and molybdenum. Even diamonds, however, are subject to wear under continuous use. Special research in this field gives sufficient evidence to assume that the wear on diamond drawing dies can be reduced to a minimum by employing the most suitable cristallographic orientation of the drawing cone.

Introduction

From a technological point of view, diamond is a most useful material since it is the hardest of all known substances. Owing to this property its value as a material for tools is unsurpassed: 80% of the yield of the diamond mines is used for industrial purposes and only 20% finds its way into the jeweller's showcase.

In this paper we shall confine ourselves to the diamond drawing dies for the manufacture of fine wire from very hard metals, such as tungsten. Dies of any other material are not suitable for drawing very hard metals into wires of small diameters except at the cost of enormous wear on the dies.

When a diamond is to be used as a drawing die, a hole of the desired profile and minimum diameter has first to be drilled through it. This can be accomplished by a special process; holes having a purely circular cross-section can be obtained in all diameters. If the diamond is to function satisfactorily as a drawing die, the minimum diameter of the hole should not change and the aperture should retain its circular shape. This ideal state, however, cannot be maintained in practice; even diamonds are subject to some wear during use. After several thousands or tens of thousands of yards of tungsten wire have passed through it, the shape of the hole is found to have changed considerably.

The extent of this wear as well as the ultimate shape of the hole depends on several factors, among which may be mentioned the condition of the outer layers of the material to be drawn, the lubricant used and the temperature. Even if these factors are kept constant, remarkable differences in the nature and the rate of wear may occur. This is due to the fact that a diamond always contains impurities and inclusions that may influence its wear. Moreover, wear will occur in different structural planes, according to the direction of the drilled hole with respect to the crystal orientation, and it is well-known that the resistance to wear of diamond depends greatly on the crystallographic orientation of the faces that are subjected to the wear.

This effect will be dealt with in this article [1]). Before considering the wear during the wire drawing process we shall give a brief summary of the resistance to wear of diamonds in general.

Effect of crystallographic orientation on the resistance to wear of diamond

In the diamond-working industry it is a well-known fact that diamonds can be ground and polished far more easily in certain directions or on certain faces than in other directions. The wear resistance of diamond shows a pronounced anisotropy and the directions of minimum wear resistance are closely related to the crystal structure.

Crystal structure

Diamond crystallizes in the cubic system. The arrangement of the carbon atoms in an elementary cell is characteristic, and other solids having a similar arrangement are often said to have the diamond structure. In such materials the binding forces between the atoms are of the valence type. They have the important property of showing pronounced preferred directions in space. The carbon atoms in the diamond lattice each have four nearest neighbours, arranged tetrahedrally around the central atom, the four bond directions being thus arranged symmetrically in space, as shown in *fig. 1*. The carbon atoms are situated at the corners and in the face-centres of a cube, as with the ordinary face-centred structure, but apart from these the cell contains another four atoms. If the cube is divided into eight similar small cubes, each having half the edge of the unit cell, then these four additional atoms (hatched in fig. 1) are to be found in the centres of four of the small cubes, which are so arranged that any two cubes have only one edge in common. The above-stated condition that any given carbon atom is tetrahedrally surrounded by four neighbours, is thus satisfied.

---

[1]) This subject will be treated in greater detail in paper a by the same authors to be published shortly in Applied scientific Research.

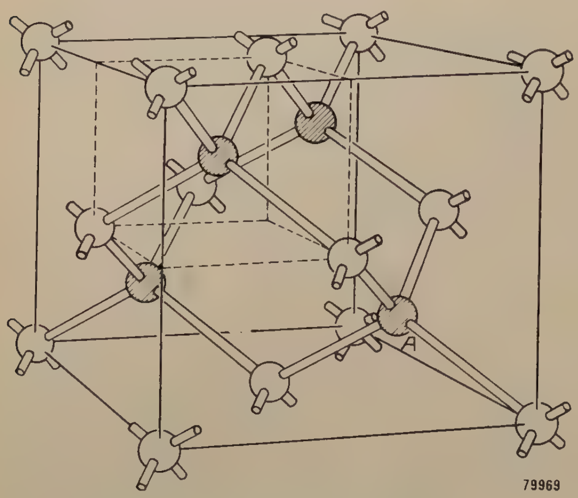

Fig. 1. Cubic unit cell of diamond.

The hardness of the diamond is largely due to the fact that great energy is required to liberate one or more carbon atoms from their tetrahedral surroundings, since this involves the breaking of several bonds and disruption of their symmetry, which is essential in valence-bond crystals.

The orientation of the boundary planes of the natural diamond is as a rule simple and nearly always occurs in three forms viz:

a. Along the cube faces, termed (100)-planes in the crystallographic notation.

b. Along the rhombic-dodecahedral faces or (110)-planes. These are planes through a cube edge and parallel to the face diagonal of a plane perpendicular to this edge.

c. Along the octahedral planes or (111)-planes, i.e. planes perpendicular to a body diagonal of the cube.

Wear

When the various diamond faces are ground (neglecting for the moment the *direction* of grinding) it is found that the three planes most commonly occurring show different wear resistance. The rhombic-dodecahedral faces are as a rule most easily ground, i.e. the material is readily removed by a force acting in the rhombic-dodecahedral plane. The cube faces are harder to deal with, and the octahedral faces are the most wear-resistant, which means that a force acting in the octahedral plane removes only very little material.

In a given plane, however, the *direction* of grinding is also of importance. Each type of plane is found to have one or more preferential directions, along which the wear resistance is smallest. In the (110)-plane this preferential direction is along the cube direction in that plane, in the (100)-plane both cube directions are equally preferential, whereas in the octahedral planes the orthogonal projections of the three cube directions in that plane are the directions of preference. *Fig.* 2 shows the fundamental orientations of minimum wear resistance: i.e. the directions along which the diamond crystal is most easily ground.

For directions other than the preferential, the ease of grinding may well be approximated by:

$$S = A \cos^2 \Theta , \quad \ldots\ldots \quad (1)$$

in which A represents a constant depending solely on the nature of the grinding plane. According to the foregoing, A will be large for (110)-planes and small for (111)-planes. Θ indicates the angle between the actual and the preferred grinding directions.

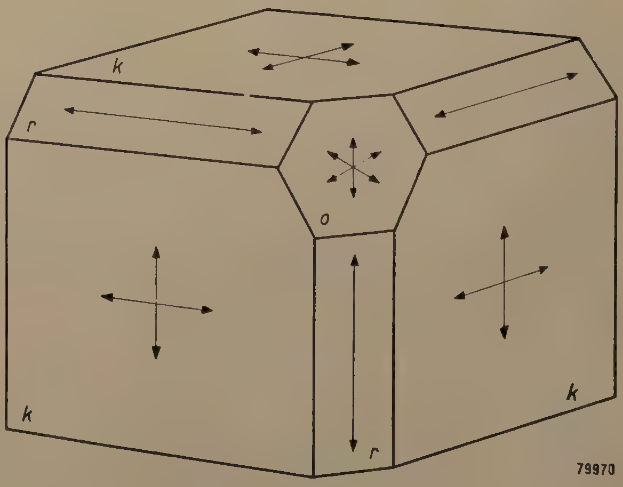

Fig. 2. Schematic diagram of preferred orientations for diamond grinding. The preferred directions on the various crystal faces are indicated by arrows whose lengths are proportional to the ease of grinding. Cube planes are indicated by *k*, rhombic-dodecahedral planes by *r*, and octahedral planes by *o*. (Diagram taken from the article referred to in [2].)

The cohesion of the atoms in a diamond crystal can be broken not only by grinding, but also by cleavage. The octahedral plane proves a favourable cleavage plane, which means that a force applied so that it acts perpendicular to the octahedral planes will effect a breaking of the bonds relatively most easily. As in the case of grinding, just the opposite applies to forces acting parallel to these planes.

The explanation of this anisotropy in diamond wear, according to Stott [2]) and others is to be found in the nature of the directional bonding forces between the atoms. As an example we shall consider here only the case of the wear resistance of the rhombic-dodecahedral plane ((110)-plane). *Fig. 3* shows the configuration of the atoms in a diamond lattice as seen from a direction at right angles to this plane. The atoms indicated by the black dots lie in the plane of the drawing, and therefore in the rhombic-dodecahedral plane to be ground; the circles show the atoms in the first layer beneath this plane. The connecting lines show the interatomic bonds; the full lines are those parallel to the plane of the drawing and the dotted lines show the bonds with the deeper layer. For the sake of clarity the atom *A* corresponds to that denoted by *A* in fig. 1. It appears that atom *A* can be more readily removed by a force in the direction of arrow *1*, i.e. in the cube direction, than by one acting along arrow *2* which is perpendicular to it. The cube direction is consequently to be preferred in grinding.

Similar considerations will satisfactorily explain other directions of preference with respect to wear and cleavage.

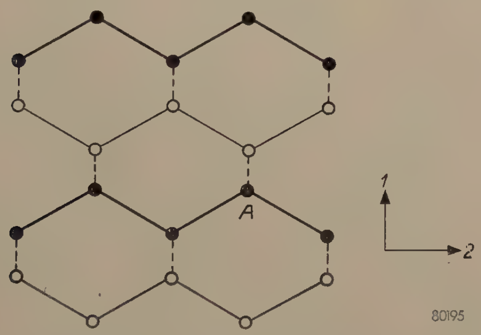

Fig. 3. Configuration of atoms in a diamond lattice as seen perpendicular to a rhombic-dodecahedral plane. The black dots represent the surface atoms in the rhombic-dodecahedral plane; the circles represent atoms in the underlying rhombic-dodecahedral plane. The full lines show the bonds parallel to the plane of the drawing, while the dotted lines represent the bonds between atoms of the two layers. Arrow *1* indicates the cubic direction, and arrow *2* the direction of a face diagonal. Atom *A* (similarly marked in fig. 1) will more easily be removed by a force parallel to arrow *1* than by a force parallel to arrow *2*. (Cf. the article referred to by [2]).)

Wear on a drilled hole in the course of the drawing process

Let us now return to the wear on the drawing dies. There is conclusive evidence to justify the assumption that the boundary surface of the effective part of the drawing hole is composed of submicroscopic elements of crystal planes belonging to each of the above-mentioned categories. Let us first consider a hole drilled in the direction of the cube edge, i.e. at right angles to a cube face. The hole will then probably be bounded by cube planes *k* and rhombic-dodecahedral planes *r* (*fig. 4.*). According to our explanation these *r*-planes, if ground in a cube direction (as occurs, in this particular case, when wire drawing), will wear faster than any other crystal plane. The rhombic-dodecahedral planes will thus show the greatest rate of wear and the hole cross-section will assume a more or less square shape. Wear of the cube faces is also implied in the assumption of this shape. As these are also relatively easily wearing the process proceeds fairly quickly.

If a hole is drilled perpendicular to a rhombic dodecahedral plane, it will be bounded by crystal planes of all the three types discussed (*fig. 5*). None of the directions of easy wear now coincides exactly with the drawing direction. To ascertain which type of plane has the quickest rate of wear, it is necessary to decide which plane has the highest value of S (equation *1*). In this case the cube faces are those subject to the greatest wear. As shown schematically in fig. 5 the aperture will gradually become oval, with the major axis perpendicular to cube faces (which implies parallel to a cube direction). The rate of wear will be slower here than in the first instance, since no grinding takes place along a preferential direction.

If the hole is drilled perpendicular to an octahedral plane, it is surrounded by rhombic-dodecahedral planes, all equivalent as regards their orientation with respect to the drawing direction

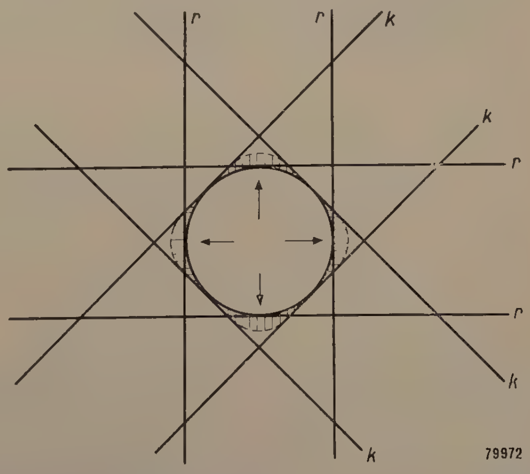

Fig. 4. A hole drilled perpendicular to a cube face is bounded by cube planes *k* and rhombic-dodecahedral faces *r*, as indicated schematically. Wear will occur mainly in the *r*-planes, so that the aperture will eventually assume a square shape.

---

[2]) W. Stott, National Physical Laboratories, Collected Reports **24**, 3-55, 1938.

(*fig. 6a*). It might, therefore, be expected that the aperture would become hexagonal, all faces showing a uniform wear. It has been found, however, that the drilled hole with this orientation often assumes a triangular cross-section.

A wholly satisfactory explanation of this phenomenon has not yet been found. It is possible that the rhombic-dodecahedral planes surrounding the hole, ultimately give way to octahedral planes (fig. 6*b*). Although not quite parallel to the drawing direction, they lie at a relatively small angle to it. The wear on these octahedral planes, half of which lie at a small positive angle and the other half at a negative angle with the drawing direction, will now apparently predominate. More wear will occur on the octahedral planes o "along" which the grinding action takes place than on those marked 0′ "into" which grinding occurs. This provides a qualitative understanding of why the aperture gradually becomes triangular. Owing to the predominance of octahedral planes and to the relatively unfavourable orientation of the grinding direction on them, the rate of wear will be very slow, much slower indeed than in the two previous cases.

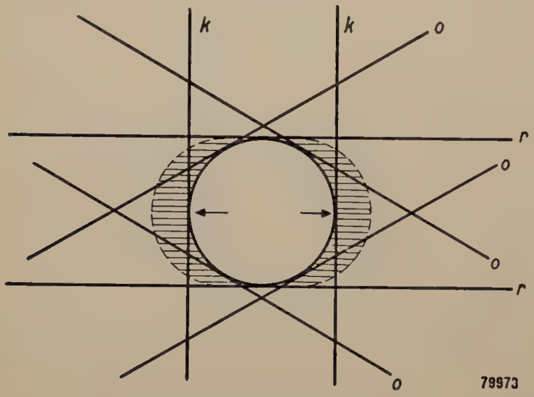

Fig. 5. A hole drilled perpendicular to a rhombic dodecahedral plane is surrounded by crystal planes of all the three main types *k*, *r* and *o* (shown schematically). Wear will occur mainly in the cube planes, so that the aperture will tend to assume an oval cross-section.

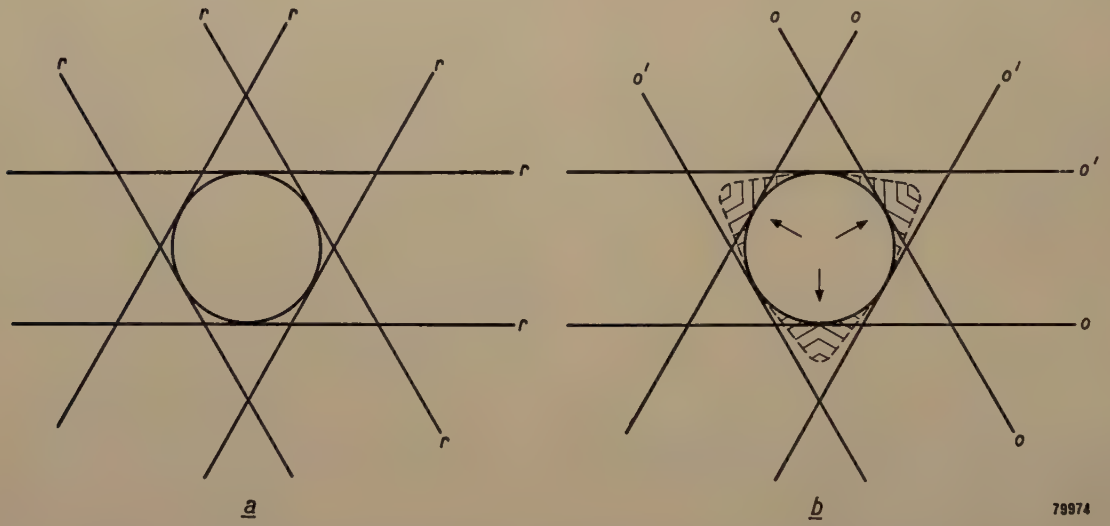

Fig. 6. *a*) A hole drilled perpendicular to an octahedral plane is surrounded by rhombic-dodecahedral planes *r*, all wearing at a uniform rate. *b*) It is supposed that, in the course of the wearing process, these planes largely give way to the octahedral planes *o* and *o*′, of which only those marked *o* will wear because of their favourable orientation with respect to the drawing direction. The ultimate cross-section of the hole will be triangular.

The conclusions regarding the symmetry of the ultimate shape of the drawing aperture can also be reached along entirely different lines of reasoning, since this shape will always be determined by the anisotropy of the diamond crystal. Drilling along a three-fold axis will produce a hole which wears to a cross-section of three-fold symmetry, etc. An altogether different matter is the *rate* of wear; information on this can only be gained by ascertaining *which* planes are being ground.

The above considerations lead to the theoretical conclusion that drawing holes should preferably be drilled as nearly as possible perpendicular to an octahedral plane in order to incur the minimum amount of wear.

Experimental research into the wear resistance as a function of the crystallographic orientation presents considerable difficulties, particularly owing to the fact that the homogeneity of diamond crystals used for wire-drawing dies is far from perfect.

Only a large-scale statistical investigation can provide the solution. For certain applications, in which large numbers of diamond dies are used, research of this kind may lead to a considerable reduction in diamond wear.

One aspect of this research may be mentioned here, viz. the determination of the orientation of a die from its X-ray diffraction pattern. The recently developed X-ray image intensifier[3]) permits of a direct visual observation of this diffraction pattern; it is no longer necessary to record it photographically.

As a further check on the above-mentioned conclusions, attemps have been made to attack diamond in a different way, namely by a process of etching or, more strictly, of burning. The results thus obtained are found to confirm the theoretical approach.

The diamond under test is fixed in a rotatable jig inside an electric furnace (*fig.* 7). The face to be etched lies horizontally and is faced at a short distance by the narrow jet nozzle of a silica tube set in a movable mount. By suitable movement of the nozzle, combined with rotation of the diamond, the whole surface of the latter can be covered. Inside the oven the temperature in maintained at 800-900 °C, whilst an atmosphere of hydrogen is supplied to prevent combustion of the diamond. A fine jet of oxygen blown out of the moving nozzle onto the diamond then has a pronounced "etching" effect (actually a burning).

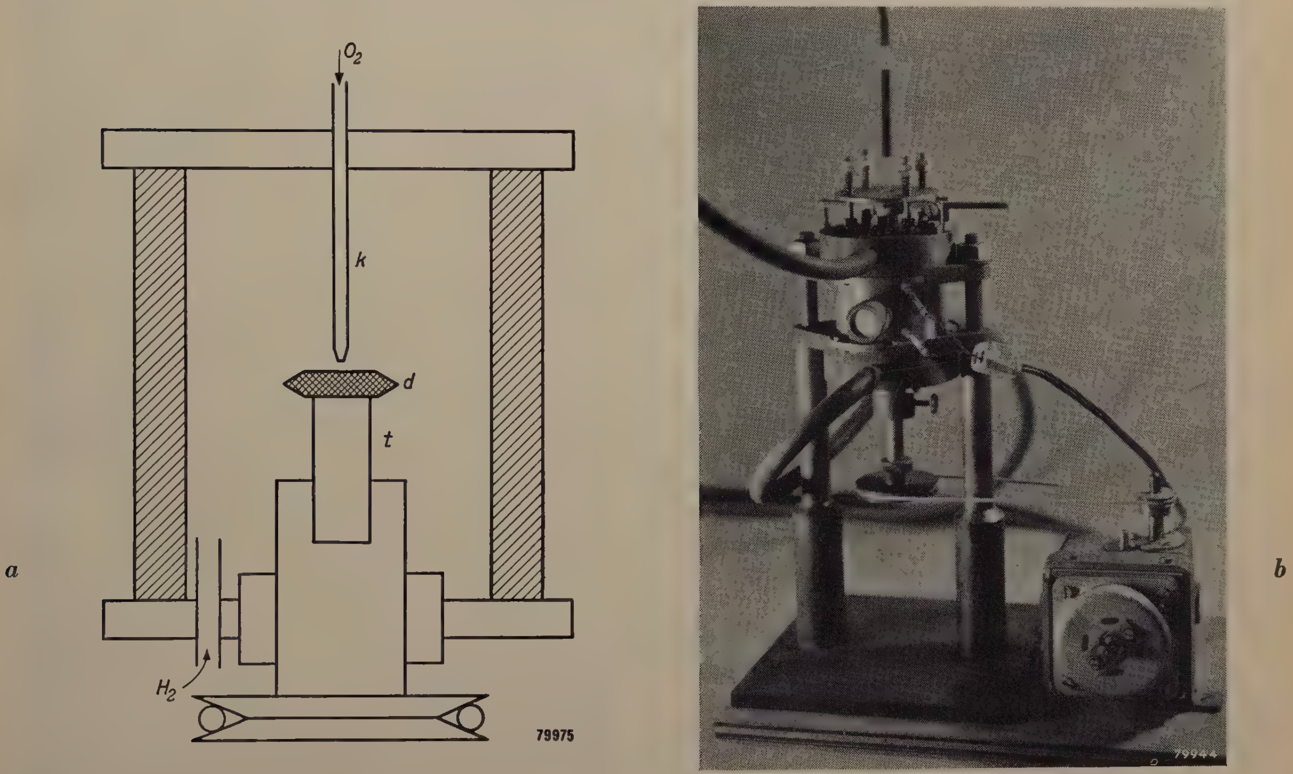

Fig. 7. *a*) Apparatus for the etching of a diamond by burning with oxygen. The diamond *d* is fitted on a rotatable table *t*. A movable silica nozzle faces the upper surface of the diamond. The whole assembly is placed inside a furnace supplied with a hydrogen atmosphere; the temperature inside the oven is approximately 850 °C. A jet of oxygen is blown onto the diamond through the silica tube.
b) Photograph of the apparatus.

Etching of diamond faces

Diamond, as is known, is totally inert to the conventional pickling and etching reagents. In order to study the etch patterns on the three main faces of diamond, a special method has therefore to be applied:

It has been found that the time required to obtain the same etching effect on a (111), a (110) and a (100)-plane is quite different. This is shown in the following table, which applies to a certain uniform depth of etching.

It is clear that the rhombic-dodecahedral plane (110) is most easily etched whilst the octahedral plane (111) presents most difficulties. The removal

---

[3]) M. C. Teves and T. Tol, Electronic intensification of fluoroscopic images Philips tech. Rev. **14**, 33-43, 1952/53.

Crystal plane	Etching time in minutes
(110)	5
(100)	8
(111)	$11^1/_2$

of carbons atoms, therefore, both by grinding and by burning, is most easily effected from the rhombic-dodecahedral plane and is most difficult from the octahedral plane.

If etching takes place with the diamond rotating and a stationary jet, so that the burning is localized, it is found that the etching patterns, formed on the various diamond faces are, of the same form as the corresponding drilled holes worn in the course of wire drawing. The etching patterns obtained are shown in *fig. 8*. The square shape of the hole burnt into the cube face can be clearly distinguished from the oval crater in the rhombic-dodecahedral face and the triangular one in the octahedral face. These symmetries are entirely similar to those shown ultimately by the drawing holes in the various orientations (figs 4, 5 and 6) and in accord with that to be expected from the crystal anisotropy.

If the completely etched surfaces are examined under the electron microscope, then the cube faces are found to be covered with quadrilateral pyramids (*fig. 9a*). The rhombic-dodecahedral faces resemble something like a Jura landscape (fig. 9*b*), but the orientation of the valleys clearly coincides with the crystal directions: the valleys are oval, with the major axes lying in the cube direction. On the octahedral faces trilateral pyramids have appeared, bounded by cube planes (fig. 9*c*).

These photographs illustrate very well what happens during a polishing or grinding process.

When grinding takes place along the (111)-plane the trilateral pyramids will soon disappear because of the comparatively easy cleavage along the (111)-planes. After all pyramids have disappeared a perfectly smooth plane is left, giving very little foothold for further grinding. The octahedral face is hence highly resistant to grinding.

On the (110)-plane new mountain ridges continue to appear because these cannot be attacked along a direction of easy cleavage and wear will continue, with a far greater uniformity. There will, however, be a great difference according to whether the grinding action occurs across or along the mountain ridges: in the latter case, wear is less readily achieved.

When a cube face isground new pyramids will continue to appear. These new pyramids cannot disappear by cleavage because no plane of easy

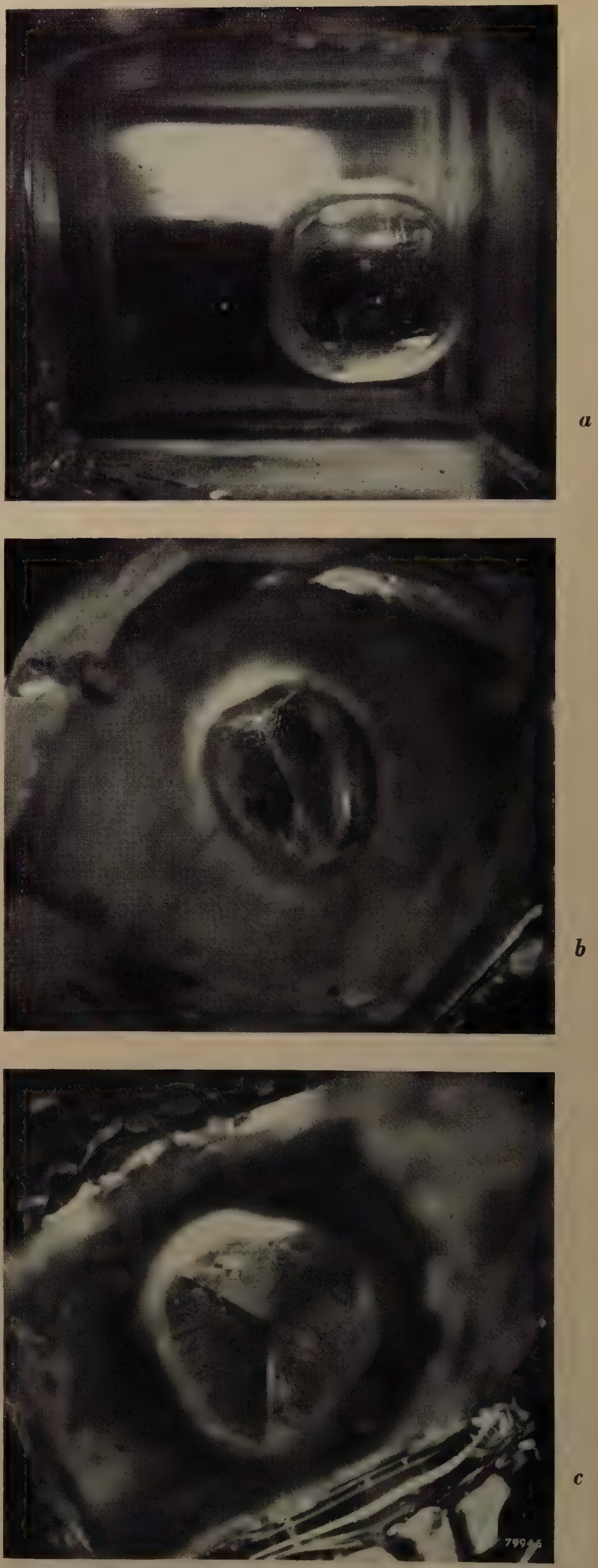

Fig. 8. Etch holes on the major planes of diamond;
a) on a cube face.
b) on a rhombic-dodecahedral face.
a) on an octahedral face.

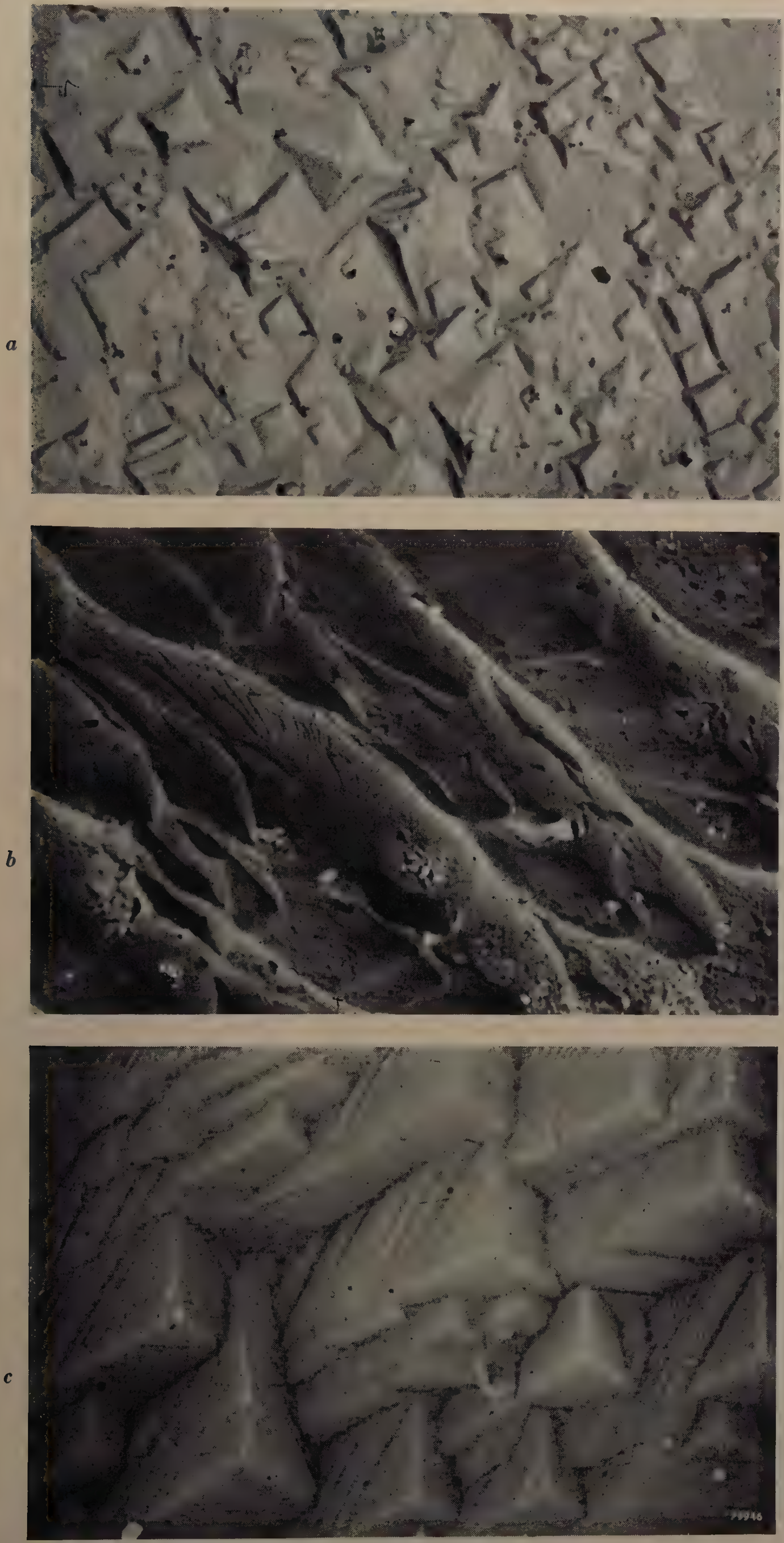

Fig. 9. Electron photo-micrographs of etched crystal faces of diamond. Enlargement 10 000 ×.
a) cube face.
b) rhombic-dodecahedral face.
c) octahedral face.

cleavage is favourably orientated. The resultant rough surface is relatively easily ground.

Summarizing, we may therefore claim that the picture obtained by etching and made visible by the electron microscope, fully confirms the theoretical picture of the wear resistance of the three major planes. Practice, however, must finally decide whether drawing dies with the theoretical optimum orientation of the hole will indeed show the least wear. As already mentioned, this will require an extensive statistical investigation, in view of the effects of factors other than the crystal orientation.

Summary. Theoretically it may be expected that the wear diamond dies will greatly depend upon the crystallographic orientation of the drilled hole, on account of the crystallographic arrangement and the special type of bond between the carbon atoms. Because of this, there are certain preferential orientations of a diamond face along which grinding is relatively more easily achieved. This is confirmed by diamond-working practice. The conclusion is reached that the least wear on a drawing die will occur if the hole is drilled perpendicular to an octahedral plane. This conclusion is checked against the etch patterns obtained by a special technique on the major faces of a diamond. Practical confirmation of these conclusions can only be obtained after a statistical examination of a great number of drawing dies.

CHEATER CIRCUITS FOR THE TESTING OF THYRATRONS

II. LIFE TESTING AT HIGH COMMUTATION FACTORS

by M. W. BROOKER *) and D. G. WARE **).

621.387:621.385.38

In Part I of the present article the authors described a "cheater circuit" which allows the measurement of the grid current of thyratrons under the full rated operating conditions, without (in the case of high-power valves) involving a large power consumption. In Part II, which now follows, the factors which control the rate of "gas clean-up" under practical conditions are considered. The more important of these are due to circuit characteristics embraced by the term "commutation factor". For thyratrons intended for industrial use, where the commutation factor may be quite high, any form of life-testing must be designed to simulate these conditions. This problem too has been solved by the use of a cheater circuit, which in this case is so designed that the test conditions to which the thyratron is subjected, are quite severe.

The causes of gas clean-up in thyratrons

For a given electrode structure in a thyratron, the gas pressure which may be used is determined by the voltage rating of the valve: for the greater the gas pressure used, the lower will be the breakdown voltage of the valve. The life of the valve, however, may be prematurely ended if the gas pressure employed is very low, because the gas is liable to disappear, by a process which is termed gas clean-up [1]). The mechanism of gas clean-up has not been accurately ascertained, but it is believed to be due to high-energy gas ions hitting the electrodes with sufficient energy to penetrate the metal surface and thus becoming trapped. Now during the operating cycle of a thyratron there are two occasions on which high-energy ions may be formed:

1) during the ionization time of the valve, if the applied voltage at the moment of firing is high, and
2) immediately after conduction has ceased, if the inverse voltage appears rapidly.

These two occasions will now be considered in more detail.

Gas clean-up occurring during the valve ionization time

If a cathode-ray oscilloscope is used to observe the waveform produced when a thyratron is operated from an A.C. source, then if conduction is initiated at the peak applied voltage, the waveform will appear as in *fig. 1.* If the frequency of the applied voltage is 50 c/s, then the time elapsing between point *A* and point *D* is 10 milliseconds. On the observed trace the portion *BC* will appear vertical and very faint, showing that the valve passes from the non-conducting state to the conducting state very rapidly. In order to measure the time elapsing between points *B* and *C*, elaborate apparatus is required. This time is called the ionization time of the valve. It depends upon the applied anode and grid voltages. For a xenon-filled valve it may be as long as 0.5 microseconds for an anode voltage of 100 V, if the grid not driven positive more than 10 V. It falls to, say, 0.1 μsec at an anode voltage of 500 V, and if the grid is driven 50 V positive, the ionization time with

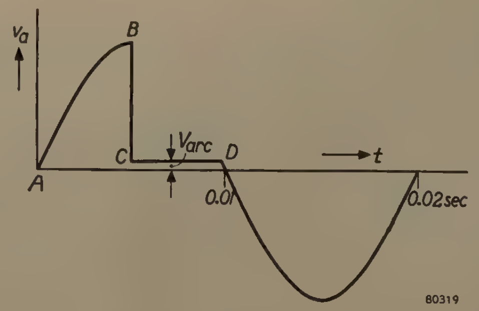

Fig. 1. Anode voltage waveform V_a of thyratron fired near peak of 50 c/s A.C. anode voltage. Ionization processes cause rapid break-down of voltage from *B* to *C*.

---

*) Mullard Radio Valve Co., Ltd., Mitcham England.

**) Formerly with Mullard Radio Valve Co., Ltd.

[1]) This refers only, of course, to valves not containing a liquid phase — e.g. mercury —, which by evaporation makes up for the vapour loss caused by clean-up. For many applications, however, this advantage of mercury is outweighed by the fact that the pressure of the (saturated) vapour rapidly increases with the ambient temperature, which imposes a strict upper limit on this temperature. In such cases, therefore, thyratrons with a gas-filling without a liquid phase are often to be preferred. As filling gases, the rare gases are commonly used, and, in special cases, hydrogen.

500 V applied to the anode may be as little as 0.01 μsec [2]).

If it were possible to observe the anode voltage and current waveforms for, say, 1 μsec after conduction is initiated, waveforms like those of *fig. 2* would be seen. It is clear, therefore, that between t_0 and t_1 (an interval of, say, 0.1 μsec) a certain number of high-energy positive ions will be produced. These positive ions will be rapidly accelerated to any negative surfaces and especially to the cathode. On colliding with a metal or glass surface an ion will have a certain probability of penetrating the surface and becoming trapped in the interior of the material. This probability becomes greater the higher the energy of the ion [3]).

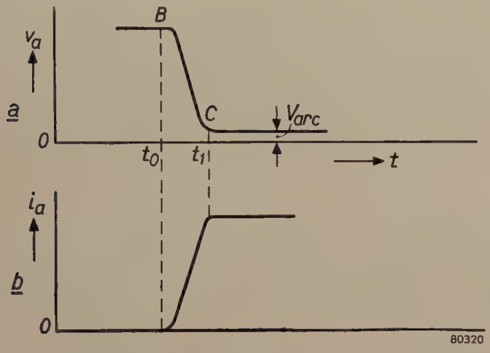

Fig. 2. *a*) Section *BC* of fig. 1, scaled-up horizontally to show gradual fall of voltage during ionization.
b) Corresponding growth of anode current i_a.

It seems probable, therefore, that gas clean-up would depend upon the type of grid excitation employed, for this in turn affects the ionization time of the valve. Thus it would appear that pulse firing of a valve would be beneficial and would produce a lower rate of gas clean-up than other forms of grid control. These expectations are confirmed in practice.

Gas clean-up occurring immediately after current extinction

A thyratron requires a considerable time after conduction has ceased for all ions present to recombine. This time is termed the de-ionization time and usually amounts to 100 μsec or more. Now it is evident that if a large negative anode voltage appears across a thyratron immediately after cessation of conduction, then the positive ions present will be accelerated to the anode and may penetrate its surface and become trapped. Thus gas clean-up may occur at current extinction by the same mechanism as at the commencement of conduction. The valve de-ionization time being long compared with the ionization time, it would appear probable that more gas would be cleaned up at current extinction than at the commencement of conduction.

However, this depends upon the waveforms of current and voltage experienced by the valve. Thus the number of ions present immediately after current extinction will depend upon the rate of decay of current prior to extinction, and the force of impact of an ion will depend on the rate of rise of the inverse voltage.

As a measure of the combined effect of these two factors in producing gas clean-up, the *commutation factor* is useful. This is a property of the circuit rather than of the valve. It can be defined as

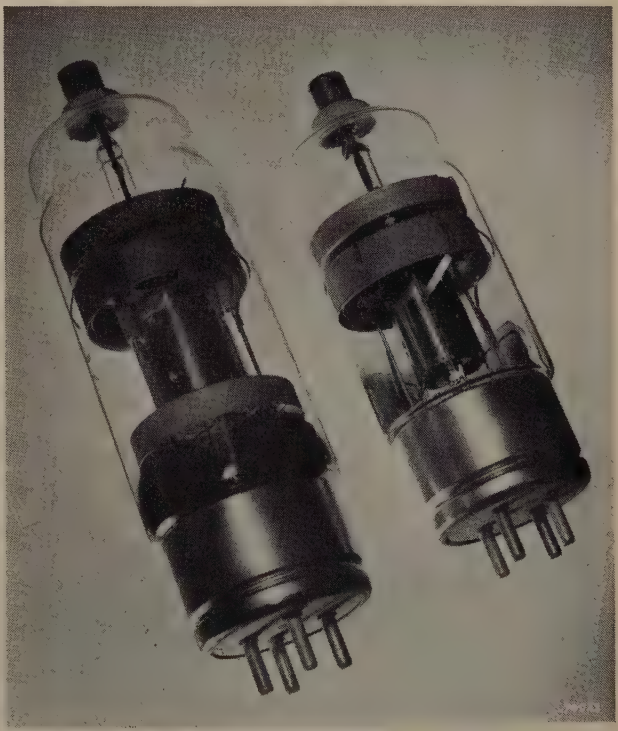

Fig. 3. Mullard thyratrons type 5544 (right) and 5545 (left) both with xenon filling and directly heated cathode. The main data are as follows:

	5544	5545
Maximum peak anode voltage		
forward	1500 V	1500 V
inverse	1500 V	1500 V
Maximum anode current		
peak	40 A	80 A
mean	3.2 A	6.4 A
Maximum commutation factor	130 $\mathrm{VA}/\mu\mathrm{s}^2$	130 $\mathrm{VA}/\mu\mathrm{s}^2$
Maximum diameter	66 mm	66 mm
Overall length	178 mm	203 mm

---

[2]) Milton Birnbaum, A method for the measurement of the ionization and de-ionization times of thyratron tubes, Trans. Amer. Inst. El. Engrs. **67-1**, 209-214, 1948.

[3]) M. J. Reddan and G. F. Rouse, A study of helium gas clean-up in an electric arc discharge, Electrical Eng. **71**, 159-164, 1952.

the product of the average rate of decay of anode current and the average rate of rise of inverse voltage, the units being amps per μsec and volts per μsec [4] [5]).

The higher the commutation factor, the more rapid the gas clean-up. A maximum value for the commutation factor is sometimes included in the published data for a thyratron. In such cases, it is obviously essential for the maker to have some simple and convenient method of life testing valves at varying rates of commutation. Such a method should make it possible to vary the rate of commutation without making major changes in the circuits. It should function when high peak currents are in use, and yet its power consumption should not be excessive. Below, a few straightforward circuits are considered in the light of these requirements, and shown to be not entirely satisfactory. A method of testing based on a "cheater" circuit is then described which has proved successful in all respects. It has been used for the operational testing of Mullard thyratrons types 5544 and 5545 (*fig. 3*; some data on these valves are given in the subscript). The present Mullard thyratrons are developed from a prototype originated elsewhere [6]).

Performance of conventional circuits

The simple circuit of *fig. 4* can meet only one of the requirements for life tests: it can produce any peak-to-mean current ratio from π upwards (π being the ratio for half sine waves, see fig. 3 of Part I [7])). It cannot, however, produce the rapid commutation which is a primary need.

If an inductance is included in the circuit (*fig. 5*). it is possible to obtain a high rate of growth of inverse voltage in the valve after conduction has ceased. Because of the lagging voltage generated in the inductance, the anode of the test valve is held positive after the applied voltage has become negative. Consequently, current continues to flow through the valve for some time. When the conduction ends, however, the inverse voltage across the valve rises abruptly to a high value, corresponding to the applied voltage. Thus, one of the causes of rapid clean-up is present; but with this circuit it is impossible to combine it with the other — a high rate of current decay.

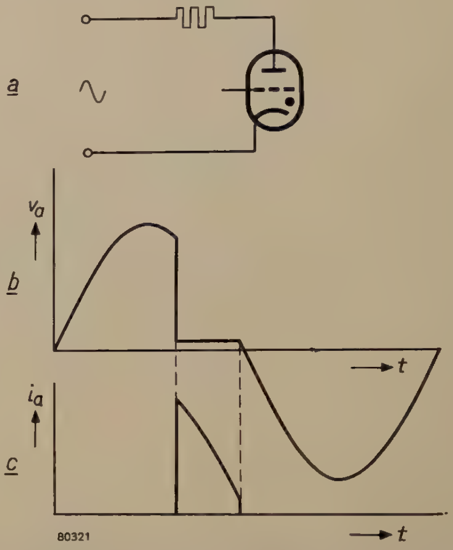

Fig. 4. *a*) Thyratron with purely resistive load. *b*) Anode voltage V_a. *c*) Anode current i_a. At current extinction both current decay and inverse voltage build-up are slow, so no high commutation factors can be obtained.

A simple two-valve full-wave circuit, with a resistance-inductance load (*fig. 6*), gets round this difficulty. The anode current flows through one valve until the other strikes. It then drops to zero almost instantaneously and the inverse voltage

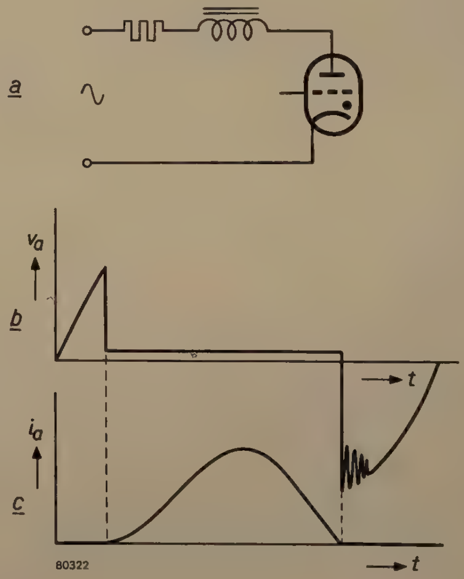

Fig. 5. With a thyratron having a partly inductive load, circuit parameters can be so chosen that conduction ceases near the negative peak of the A.C. voltage. The current decay, however, is slow, so the commutation factor is still not very high. (At current extinction, oscillations are set up in the circuit formed by the inductance and stray capacitance.)

---

[4]) Normally commutation factor is calculated by taking as averageing time of current decay the last 10 μsec before extinction, and as averageing time of inverse voltage rise the interval in which this voltage rises from 0 to 200 V.

[5]) D. V. Edwards and E. K. Smith, Circuit cushioning of gas-filled grid-controlled rectifiers, Trans. Amer. Inst. El. Engrs. **65**, 640-643, 1946. D. E. Marshall and C. L. Shackelford, Commutation factor in thyratron circuit design, Electronics **27**, 198, March 1954.

[6]) A. W. Coolidge Jr., A new line of thyratrons, Trans. Amer. Inst. El .Engrs. **67-1**, 723-727, 1948.

[7]) M. W. Brooker and D. G. Ware, Cheater circuits for the testing of thyratrons, I. Measurement of grid current, Philips tech. Rev. **16**, 43-48, 1954/55, (No. 2).

climbs quickly to its peak. Thus the commutation is extremely rapid. However, there remain two important drawbacks to the use of this circuit. Firstly, the peak-to-mean current ratio is only slightly more than two. Secondly, its power consumption is high, for it is not possible to obtain a high inverse voltage from it while using low-voltage supply.

The simplest conventional circuit that can give both speedy commutation and an adequate peak anode current appears to be a six-valve hexaphase circuit. But there is a serious objection to this as a piece of operational test gear: in the case of six fully loaded type 5545 thyratrons, for example, about 55 kW of power would be dissipated.

It is clear that no simple conventional circuit is suitable for the life testing of thyratrons at high rats of commutation. Once again, a "cheater circuit" has been devised, which permits both rapid commutation and low power consumption.

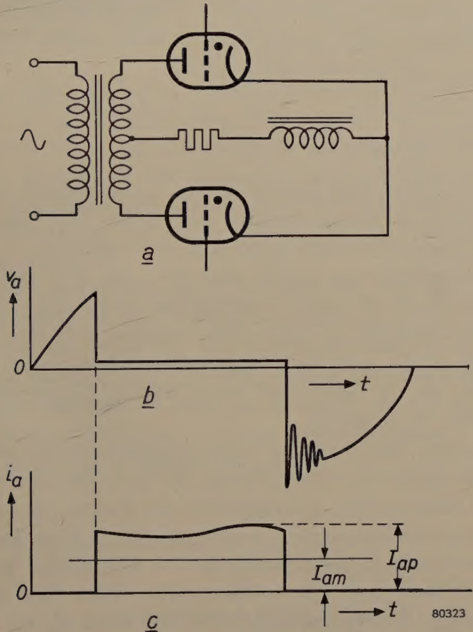

Fig. 6. *a*) Two thyratrons in full-wave circuit with resistance-inductance load. Both inverse voltage rise (*b*) and current decay (*c*) are rapid, but peak-to-mean anode current ratio I_{ap}/I_{am} hardly exceeds 2, and power consumption is high.

Cheater circuit details

An apparatus will now be described which has been used for testing type 5545 thyratrons.

In this circuit the high commutation factor required is obtained by feeding a short pulse of high negative voltage to the anode of the test valve while it is conducting. This causes a sudden break in conduction; the current falls rapidly to zero and an inverse voltage builds up at a very high rate.

The fundamentals of the circuit are shown in *fig. 7a*. The thyratron under test, Th_1, is operated from a 220 V A.C. supply. Its mean anode current can be varied by adjusting the load resistor R_1, and the grid control (which will be described later) is so arranged as to give the correct peak-to-mean anode current ratio. The rest of the circuit shown has only one function: to produce the pulses of negative voltage at the anode of the test valve. These pulses are drawn from the 1000 V transformer winding which produces a voltage in anti-phase with the mains voltage.

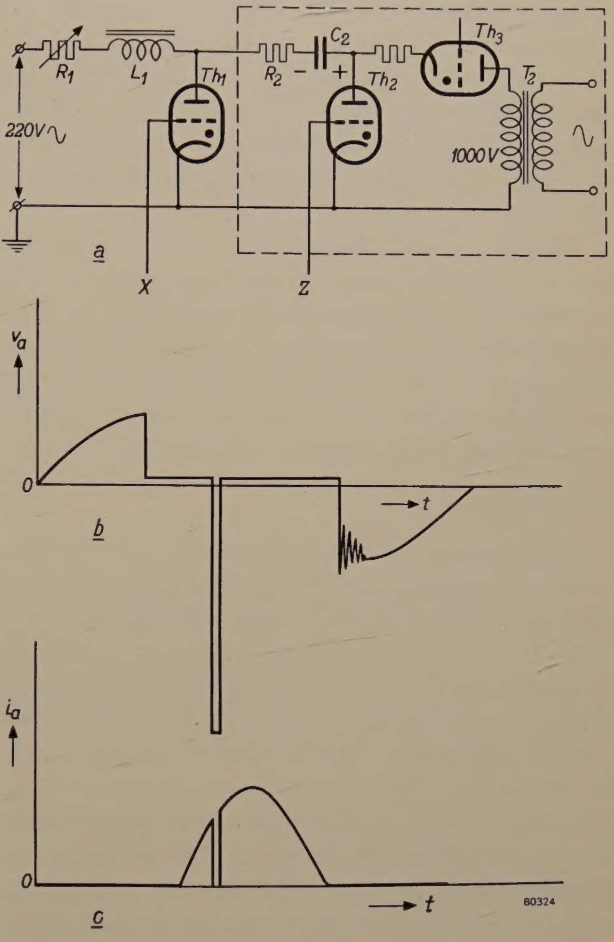

Fig. 7. *a*) Cheater circuit for thyratron testing at very high commutation factors. Th_1 valve under test, with resistance-inductance load R_1-L_1. The dotted line encloses a circuit for producing high negative voltage pulses at the anode of Th_1 that extinguish Th_1. This circuit comprises capacitor C_2 charged to approx. 1500 V from H.T. transformer T_2 via thyratron Th_3. When thyratron Th_2 is triggered, C_2 discharges through Th_1 (which is then conducting) and Th_2. Valve Th_1 is extinguished by the discharge, as shown by voltage and current waveforms for Th_1, at (*b*) and (*c*).

The sequence of events in the circuit is as follows. While the test thyratron Th_1 and an auxiliary thyratron Th_2 are not conducting, the capacitor C_2 is charged via a second auxiliary thyratron Th_3

it reaches approximately +1500 V with respect to neutral. When the flow of current through Th_3 has ceased, the test valve Th_1 is triggered. Then, while Th_1 is conducting, Th_2 is triggered. This completes the circuit of the capacitor C_2, which immediately discharges via the resistor R_2 and the valves Th_1 and Th_2.

The result is that suddenly the anode of the test valve is driven 1500 V negative (fig. 7*b*) and the flow of current through it is stopped abruptly (fig. 7*c*). Thus an extremely rapid decay of current and growth of inverse voltage occur simultaneously at Th_1, i.e., a high commutation factor has been obtained.

Whether or not the valve resumes conduction as the negative pulse decays, depends on the de-ionization time of the valve and on the method of control. However, this does not affect the operation of the test circuit, and neither would a resumed conduction unduly increase the power consumption, as the supply voltage is low.

Snubber circuits

Using the procedure described above, the commutation factor was found far too high for the original purpose, in fact it was about 10 000 VA/μsec², instead of the 80 VA/μsec² required. A special "snubber circuit", or "cushioning circuit", was therefore introduced into the apparatus to limit the commutation factor (see the first article mentioned in footnote [5]). The use of the normal resistor-capacitor combination in this rôle proved impracticable because the amount of energy available in the capacitor was so limited. Instead, therefore, an inductor L_3 and a capacitor C_3 were employed as in *fig. 8a*. They form a series resonant circuit via Th_2 while Th_1 is conducting. The voltage which appears across the test valve Th_1 as a result of this is shown in fig. 8*b*.

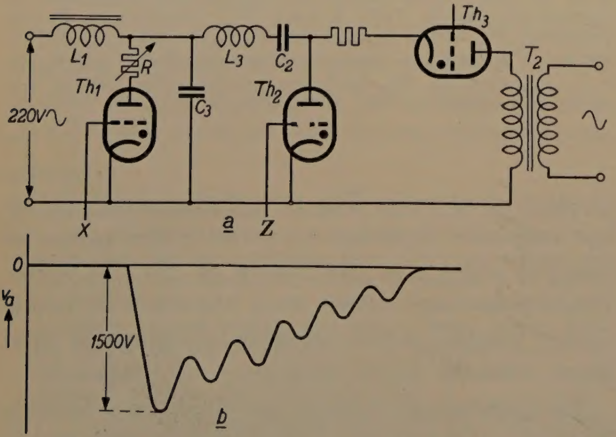

Fig. 8. *a*) Cheater circuit as in fig. 7*a*, but with "snubber" circuit L_3-C_3 for limiting the commutation factor to 80 VA/μsec². *b*) Voltage v_a appearing across the test valve.

Owing to the oscillatory nature of the discharge, the inverse voltage rises higher than it would if oscillations were absent; a peak inverse voltage of 1500 V is easily produced.

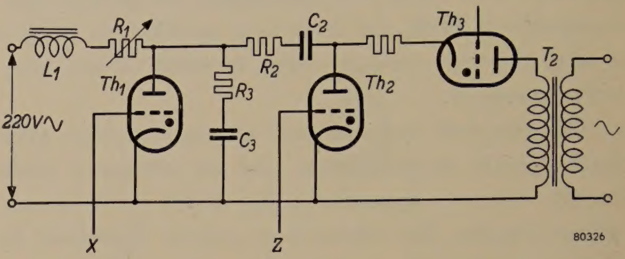

Fig. 9. Cheater circuit as in fig. 7*a*, but with an *RC* snubber circuit (R_3-C_3), used when commutation factors higher than 80 VA/μsec² are required.

Using a suitable snubber circuit, it proved possible to obtain the required commutation factor of 80 — a current decay rate of 2 A/μsec and an inverse voltage rise of 40 V/μsec. When later higher commutation factors were required, they were obtained by reverting to the usual resistor-capacitor snubber circuit (*fig. 9*).

Grid control requirements

Three separate grid control circuits were required, one for each thyratron. Taking first the test valve, Th_1, there were two important conditions which had to be fulfilled.

Firstly, it was undesirable that the grid of a type 5545 thyratron should be positive with respect to the cathode while the anode was highly negative. This would lead to a sustained discharge to the grid, and the positive ions produced would be drawn to the anode and might lead to undue clean-up or possibly to arc-back.

Secondly, it was necessary to guard against certain unwanted effects likely to be met during the early development of the 5545 thyratron i.e., grid emission and leakage troubles.

To ensure stable operation despite these defects in the valve, it seemed wisest to use a large negative bias on the grid and to trigger the valve with a short pulse. With this aim the circuit of *fig. 10* was employed. The first stage of this circuit is identical to that of fig. 6 of Part I [7]), but now a cathode follower is used as an output stage, from which pulses are fed to the grid of Th_1.

The grid control requirements of thyratron Th_2 were settled by the need to prevent conduction in Th_2 at the same time as in Th_3, i.e., the grid of Th_2 must be negative before the start of the positive half cycle of the H.T. transformer, and the grid must remain negative until some period during the conduction of Th_1. This was obtained by the use of a D.C. bias with a trigger pulse fed from a flip-flop circuit as shown in *fig. 11*. This circuit is stable with section *1* extinguished and section *2* conducting. The trigger pulse from the circuit shown in fig. 10 is used to render section *1* conducting and to extinguish section *2*. The variable resistor R_6 is used to vary the period during which section *2* is extinguished. When section *1* is extinguished again, a positive pulse is fed to a cathode-follower, and from thence (point *Z*) to the grid of Th_2. A choke is connected in the cathode circuit of the final stage of this grid pulse network, thus reducing the rate of rise of current through the cathode-follower. This ensures that an oscilloscope can be triggered (from point *U*) before the grid of Th_2 becomes sufficiently positive to produce conduction. In this way the whole period of current decay and inverse voltage rise can be observed on the oscilloscope. The cathode-ray oscilloscope trigger is a necessity in order to avoid "jitter", but even so it is difficult to observe the oscilloscope trace for periods of one or two microseconds after the time of current extinction, due to the transient effects of stray capacitances and inductances.

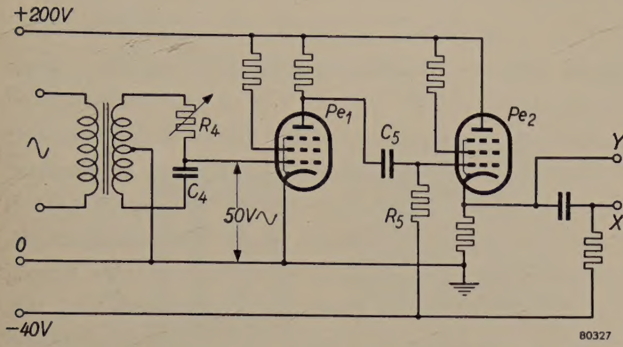

Fig. 10. Circuit for supplying triggering pulses, Pentode Pe_1 is strongly overloaded by A.C. grid voltage of 50 V, 50 c/s, (derived from phase-shifting network R_4-C_4), so that square-wave anode current is produced. This waveform is differentiated by C_5-R_5, giving positive and negative pulses. The positive pulses control a cathode-follower (pentode Pe_2). Terminal *X* is connected to grid of test valve (Th_1 in figs. 7*a*, 8*a* and 9), terminal *Y* to a flip-flop (fig. 11) firing auxiliary valve Th_2.

For the capacitor-charging thyratron Th_3 the grid control circuit is much simpler. The main requirement is that it should not trigger Th_3 until Th_2 has had ample time to de-ionize; otherwise the capacitor C_2 would be short-circuited and would not charge properly. A delay of about 60° in the triggering of Th_3 is enough for this purpose, and it is obtained by the use of a simple phase-shifting network.

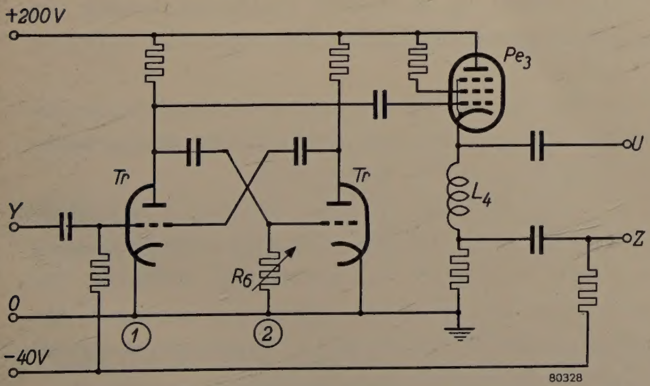

Fig. 11. Flip-flop circuit. It is stable with section *1* of *Tr* (Mullard ECC 33 double triode) non-conducting, section *2* conducting. A positive pulse at *Y* (from circuit shown in fig. 10) trips the flip-flop, which returns to stable position after a time variable by resistor R_6. The cathode-follower output stage contains the pentode Pe_3. The pulse appearing at terminal *U* triggers the oscilloscope, while the pulse at *Z* fires the auxiliary thyratron Th_2 (figs. 7*a*, 8*a* and 9). Choke L_4 ensures that the pulse at *U* appears earlier than the pulse at *Z*.

Results obtained with the cheater circuit

The apparatus has been used to life-test valves of type 5545 for periods up to 2200 hours. This is quite a considerable time, taking into account that the valves were run at commutation factors of 450-750 VA/μsec², i.e., several times the published valve rating (130 VA/μsec²). Special valves were made with pressure gauges attached comprising a quartz fibre, which could be set into vibration. The damping of this vibration is a measure of the gas pressure in the valve. Using such gauges, the gas pressure could be measured at intervals throughout the life of the valve.

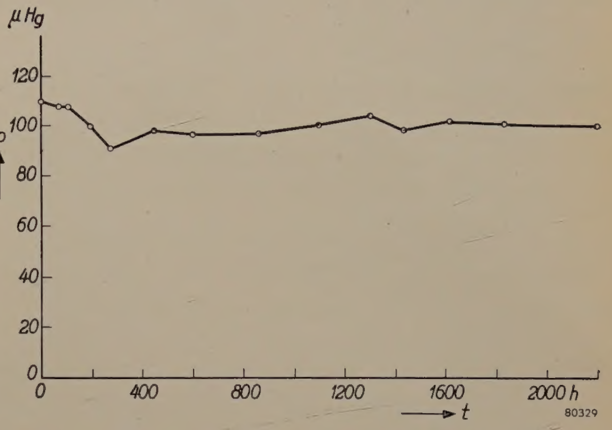

Fig. 12. Gas pressure *p* in xenon-filled Mullard MT 5545 thyratron during a test for gas clean-up. The first 1270 hours the valve was run with a commutation factor $f_c = 450$ VA/μsec², the rest of the time with $f_c = 750$ VA/μsec².

The results obtained with a valve of type 5545 are shown in *fig. 12*. The accuracy of the measurements is about 5%. It can be seen that a small amount of gas clean-up occurs during the first 250 hours and thereafter the gas pressure remains substantially constant. These characteristics were maintained even at commutation factors as high as 750 VA/μsec².

Work is in progress on other valve types to compare the suitability of various valve structures, but the above results already bear out the claims made for this valve construction by its designers [6]).

Summary. The life of a thyratron may be unduly shortened by gas clean-up. This effect is strongest when the commutation factor (product of rate of current decay and rate of inverse voltage built-up) is high. The need was felt, therefore, for life tests at a high commutation factor. However, conventional circuits satisfying this condition have a power consumption which with large thyratrons is almost prohibitive. This difficulty was circumvented by the use of a "cheater circuit" that simulates the desired working conditions with a great economy of power. A life test of a xenon-filled Mullard MT 5545 thyratron in such a circuit is discussed. There appears to be no appreciable gas clean-up in over 2000 hours, at commutation factors up to 750 VA/μsec², which is far in excess of the published valve rating.

ABSTRACTS OF RECENT SCIENTIFIC PUBLICATIONS OF N.V. PHILIPS' GLOEILAMPENFABRIEKEN

Reprints of these papers not marked with an asterisk * can be obtained free of charge upon application to Philips Electrical Ltd., Century House, Shaftesbury Avenue, London W.C. 2.

2089: J. I. de Jong and J. de Jonge: The action of bromine on derivatives of urea in neutral aqueous solution (Rec. Trav. chim. Pays-Bas **72**, 169-172, 1953).

It was found that only unsubstituted amide groups in derivatives of urea are rapidly attacked by bromine in neutral solution, while the reactions with alkylated amide groups is very slow. Dimethylol urea has a symmetrical structure.

2090: K. H. Klaassens and C. J. Schoot: Derivatives of p-diethoxybenzene, II. 1,4-diethoxy-2-aminobenzene-5-diazoniumborofluoride (Rec. Trav. chim. Pays-Bas **72**, 178-182, 1953).

The preparation of the compound named above is described and its structure is confirmed.

2091: Y. Haven: Dielectric losses in sodium chloride crystals (J. chem. Phys. **21**, 171-172, 1953, No. 1).

By plotting log (tan δ) against log frequency it is possible to distinguish between dipole losses (Debye losses) and conductivity losses. Measurements were made at 100 °C on very pure NaCl and on contaminated NaCl (0.003 mole percent divalent ions, 0.05 mole % Ca^{2+}, 0.14 mole % Ca^{2+}, 0.008 mole % Mn^{2+}, and 0.014 mole % Mn^{2+}). The Debye losses appear to increase with increasing contamination.

2092*: H. P. J. Wijn: Magnetic relaxation and resonance phenomena in ferrites (Thesis, Leiden 1953).

After a short review of the preparation and properties of sintered ferrites (Ch. 1), the measuring methods are described that have been used to determine the magnetization curves and the distortion as a function of frequency. The conditions that must be fulfilled in order to limit the systematic error in the measuring results are discussed. For ferrites with a high initial permeability the magnetization curve depends on frequency such that, up to rather high inductions, there is a linear relation between the induction and the magnetic field in the ferrite. This frequency dependence is not found for ferrites having an initial permeability below about 400, unless they are fired at a very high temperature (1500 °C). In Ch. 4 the influence of porosity and external stresses on the magnetization curve is examined, and the conclusion is reached that when (at high frequency) a magnetization curve becomes a straight line, the irreversible domain-wall displacements no longer take place. Ch. 5 deals with the frequency dependence of the initial permeability of ferrites and it was established that at high frequency a resonance phenomenon underlies the decrease of the permeability. Moreover a ferromagnetic resonance of the type described by Snoek is found for a ferrite under a large external stress such that only simultaneous spin rotations make a contribution to the permeability. The resonance frequency is related in a simple way to the natural ferromagnetic resonance frequency of the same ferrite. In this chapter some results of measurements are also given that point to a new relaxation phenomenon, which is largely responsible for the residual losses in ferrites.

After a brief survey of the theories found in the literature concerning the dispersion mechanism of domain wall displacements and spin rotations in Ch. 6, the next chapter compares the measured results with these theories. The following conclusions are reached:

a. The relaxation of irreversible domain-wall displacements is brought about by a friction process characterized by a friction coefficient having the order of magnitude of unity. The origin of this friction is unknown.

b. The theory of ferromagnetic resonance permits many of the properties of the initial permeability at high frequency to be clarified.

c. The relaxation process causing a dispersion in the initial permeability of ferrites at low frequency is closely connected with an electron diffusion. The activation energy of this relaxation process is the same as that found from the temperature dependence of the resistivity of ferrites.

Though in some ferrites at high frequency *B* is a linear function of *H*, it is seen in the last chapter that many losses still occur in the ferrite, giving rise to a phase shift between field and induction. Finally it is shown that in the case of ferrites, the determination of the distortion from the hysteresis loss can give erroneous results.